From **The Department of Clinical Science, Intervention and Technology**
Division of Audiology
Karolinska Institutet, Stockholm, Sweden

THYROID HORMONE MEDIATES FIBROBLAST GROWTH FACTOR RECEPTOR EXPRESSION, WHICH BOTH ALTER CELL SURFACE MECHANICAL PROPERTIES OF THE MAMMALIAN COCHLEA

Katherine B. Szarama

Karolinska Institutet

Stockholm 2012

Published by Karolinska Institutet.

ISBN 978-91-7457-930-7

Printed by
REPROPRINT AB
Stockholm 2012
www.reproprint.se
Gårdsvägen 4, 169 70 Solna

This thesis is dedicated to my brother, Daniel.

ABSTRACT

Cells in the mammalian hearing organ, the cochlea, develop a specialized patterning and cellular architecture necessary for hearing function. Cytoskeletal components, such as actin and microtubules, maintain the material and mechanical properties of these cells. One way to understand cell material properties is to measure the response of the cytoskeleton to mechanical stress. Mechanical stress to sensory hair cells and non-sensory supporting cells in the cochlear epithelium, the organ of Corti, can lead to hearing loss, and currently these cells cannot recover from cytoskeletal damage. Quantification of the mechanical properties of these cells as they develop is lacking. By understanding cytoskeletal development, it may be possible to repair damaged cells to restore hearing function.

Using Atomic Force Microscopy, we measured cell surface mechanical properties in cochlear tissue culture during development. We calculated and compared the Young's modulus of sensory outer hair cells (OHCs) and non-sensory supporting pillar cells (PCs) at discrete time points between embryonic day 16 (E16) and postnatal day 5 (P5). We find the first distinctions between OHC and PC Young's modulus in the late embryonic period, after E16. By P5, PCs have developed a network of acetylated microtubules that occupy the majority of PC cytoplasm, which may in part explain the higher Young's modulus and increased stiffness relative to OHCs, which are primarily composed of actin filaments at the lumenal surface.

To understand the growth factors regulating cochlear cellular development after E16, we antagonized both the Fibroblast growth factor (Fgf) and thyroid hormone (TH) signaling pathways. Using an in vivo mouse model, we find that loss of Fgfr3 leads to a decrease in the Young's modulus of both OHCs and PCs, which suggest that the disruptions to tissue architecture may contribute to the hearing loss in these animals. To disrupt TH levels in the cochlea, timed-pregnant female mice were treated with methimazole to induce a hypothyroid state *in utero*. We find that hypothyroid cochleae have a delay in down regulation of Fgfr3 in OHCs and disruptions to OHC and PC morphology. Interestingly, OHCs and PCs are stiffer in hypothyroid relative to control conditions. By examining both the transcriptional profile and the Fgf-signaling cascade, we find that the aberrant cellular stiffening results in part from persistent activation of Fgf-receptors and the actin depolymerizing factor cofilin.

Finally, we wanted to examine the morphology and mechanics of OHCs and PCs before they are fully differentiated. Using immunohistochemistry and confocal microscopy, we find that overlap of prosensory specific markers, including Islet1, Sox2, and Jagged1, may help to refine the population of prosensory cells that will give rise to the organ of Corti. Defining this region may permit quantification of prosensory cell surface mechanical properties in the un-differentiated sensory epithelium. Together, these data suggest that growth factors impact the developing OHC and PC cytoskeleton, which dictates cell surface mechanical properties during development. By understanding the material properties of these cell types, future research may consider manipulation of growth factor signaling pathways to repair the organ of Corti in order to restore hearing function.

LIST OF PUBLICATIONS

This thesis is based on the following publications:

I. Szarama KB, Gavara N, Petralia RS, Kelley MW, Chadwick RS. Cytoskeletal changes in actin and microtubules underlie the developing surface mechanical properties of sensory and supporting cells in the mouse cochlea. *Development.* 2012 Jun; 139(12):2187-2197.

II. Szarama KB, Stepanyan R, Petralia RS, Gavara N, Frolenkov GI, Kelley MW, Chadwick RS. Fibroblast growth factor receptor 3 regulates microtubule formation and cell surface mechanical properties in the developing organ of Corti. *BioArchitecture*. 2012 November/December; 2(6):1-6.

III. Szarama KB, Gavara N, Petralia RS, Chadwick RS, Kelley MW. Thyroid hormone increases Fibroblast Growth Factor Receptor activity and disrupts cell mechanics in the developing organ of Corti. Submitted to BioMedCentral's *Developmental Biology*.

IV. Kelley MW, Chu J, Isgrig K, Szarama KB, Puligilla C, Coate TM. Localization of prosensory and sensory domains within the developing cochlear duct. *Manuscript.*

CONTENTS

LIST OF FIGURES

LIST OF ABBREVIATIONS

D	Deiodinase selenoenzyme
DMSO	Dimethyl sulfoxide
DNA	Deoxyribonucleic acid
E	Embryonic day
F	Fibroblast growth factor
GTP	Guanosine-5'-triphosphate
MAPK	Mitogen-activated protein kinase
L	Leucine
OHC	Outer hair cell
P	Postnatal day
PBS	Phosphate buffered saline
PC	Pillar cell
PI3K	Phosphoinositide 3-kinase
PLC-γ	Phospholipase C gamma
Prox1	Prospero-homeobox transcription factor 1
RNA	Ribonucleic acid
rT3	reverse triiodothyronine
RXR	Retinoid X Receptor
Sox2	Sex-determining-region-Y box transcription factor 2
STAT	Signal Transducer and Activator of Transcription
T3	Triiodothyronine
T4	Thyroxine
TR	Thyroid hormone receptor
TRE	Thyroid hormone response element
Ym	Young's modulus

1 INTRODUCTION

Hearing loss is partly due to the inability to repair or regenerate damaged inner ear sensory hair cells or non-sensory supporting cells. By understanding morphogenesis in the inner ear sensory epithelium, the cochlea, we may be able to apply the mechanisms of development to therapeutic interventions for hearing loss. One obstacle to manipulating developmental processes is the lack of understanding of the contribution of cytoskeletal components that resist cellular deformations, during development or through the process of hearing. If we can better understand the mechanics of development, then we can potentially manipulate those mechanisms to facilitate repair or regeneration.

1.1 CELL MECHANICS AND MORPHOGENESIS

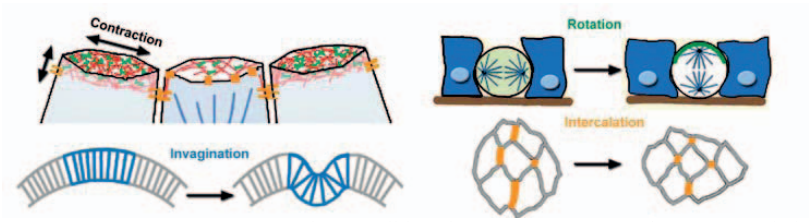

Figure 1. Tissue Morphogenesis. Examples of cell-based events in tissue morphogenesis, including contraction, rotation, invagination, and intercalation. These changes in cell shape are induced by apically driven changes in cytoskeletal components, such as actin (red), myosin (green), microtubules (blue) and cell-cell junctions (yellow). Figure adapted from Martin and Gelbart, 2010; Gillies and Cabernard, 2011; Gorfinkiel and Blanchard, 2011; Levayer and Lecuit, 2012.

Cell shape changes and movements are part of the growth and maturation of tissues throughout the body. Epithelial morphogenesis includes the re-distribution of forces during cell shape changes. These tissue movements (**Figure 1**) can be described at the cellular level as contraction, invagination, intercalation, and rotation (Levayer and Lecuit, 2012). Furthermore, changes in cell shape often manifest changes in the material properties of the cell, such as the stiffness or elasticity. Stiffness is a material's resistance to deformation by applied force. This is an extensive property of a given structure dependent on both the material shape and constituent components. Elasticity is the material property by which a structure can return to a resting shape after deformation, which is defined as stress or strain. Cells also have a fluid component, and the resistance to deformation of a fluid is termed viscosity. It is for this reason that cells are often referred to as viscoelastic, since cell contents can also behave like a viscous fluid. Quantitative descriptions of cell mechanical properties may lend insight into these cell shape changes.

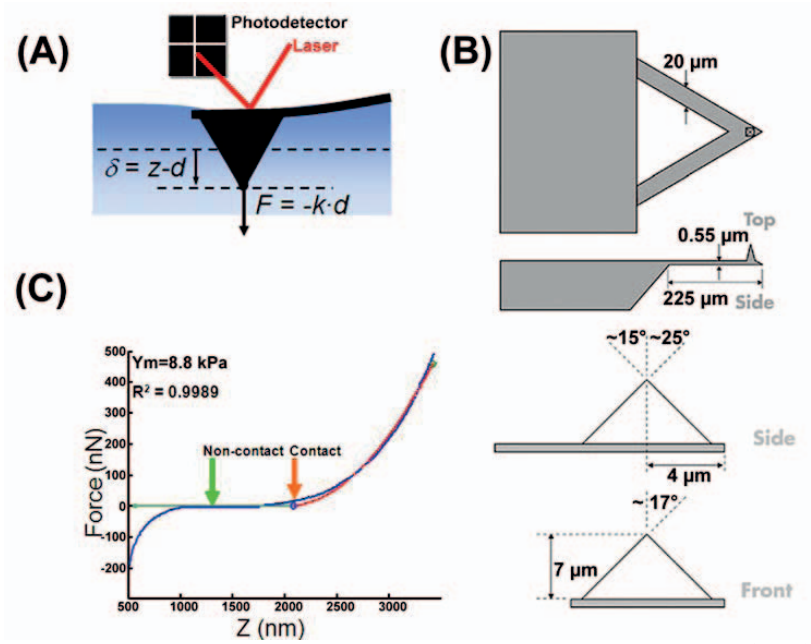

Figure 2. Atomic Force Microscopy (AFM) to be applied to cell morphogenesis. (A) Schematic of AFM stiffness measurement with cantilever in contact with the sample surface (blue). Position of cantilever is monitored by tracking a laser reflected off the surface of the cantilever and onto a photodiode detector. The force (F) applied by the cantilever is a function of the cantilever spring constant (k) and distance (d) traveled by the cantilever. The photodiode can detect the displacement (δ), which includes both the distance and the indentation of the sample (z). (B) Tip dimensions for gold-coated silicon nitride cantilever (Bruker Nanoprobes) used in AFM experiments. µm, micrometer. (C) Sample force-distance curve (blue). The force-distance curve contains three parts, a non-contact region (green line), and a contact point (orange arrow). The contact region of the curve is analyzed by applying non-linear least-squared fit (red) to estimate Young's modulus (Ym). The force-distance curve shown has a goodness of fit (R^2) value equal to 0.9989. nm, nanometer; nN, nano-Newton.

One measurement of cell mechanical properties is the Young's modulus (Ym). This elastic modulus is an intensive property independent of changes in shape. A lower Ym is a desirable property of a material when higher flexibility is necessary. One way to measure Ym is to adapt optical microscopy to include applications of controlled force. The atomic force microscope (AFM) places a microscopic cantilever probe (Figure 2) in contact with a cell or tissue sample in order to apply a wide range of forces (10 pN to N) over several scales in length (50 nm to 10 µm). Movements of a laser reflected from the cantilever probe onto a detector provide a minimally invasive technique that does not require fixation (Figure 2). The high resolution for both imaging and force measurements requires a sharp AFM probe. One constraint of the surface area of the tip shape is a greater exertion of stress (σ = Force/Area), which can be corrected through optimization of the cantilever's shape for the desired experiment. In summary, application of AFM allows quantification of the changes in cell mechanics and may directly influence tissue development.

To extract Ym from AFM measurements, the data must be fit to the applicable model (Figure 2). The force on a rigid cone indenting an elastic half-space was modeled by Sneddon and Love (Love, 1939; Sneddon, 1965). These, and subsequent specifications thereafter assume that for a cantilever of known stiffness, the amount of deformation is dependent on the elastic modulus of the material in contact (see

Appendix I). This model also assumes that the sample is linearly elastic, homogeneous, and isotropic, and that indentation depth is small relative to the height of the sample. Further solutions account for special deviations considering AFM probe geometry, (Bilodeau, 1992; Briscoe et al., 1994). More recently, additional considerations to optimize the use of AFM to estimate the Ym of biological samples (Dimitriadis et al., 2002) has been followed by an increasing interest in understanding the mechanical properties of stem cells (Yim et al., 2010) or scaffolds thought to guide directed cell behaviors (Sundararaghavan et al., 2011), both of which may provide quantitative data that help to describe the developmental time course of cells and tissues.

The shape changes observed during epithelial morphogenesis are driven largely by the apically concentrated cytoskeletal components, actin and non-muscle myosin (NM). The motor activity of NM-II increases fluidity, which is the opposite of viscosity, in poorly cross-linked actin (Koenderink et al., 2009), while NM-II motor activity increases stiffness in highly cross-linked actin (Humphrey et al., 2002). This suggests that decreasing NM-II activity could have different effects in neighboring cells based on the extent of cross-linking. Also, turnover in actin filaments has been shown to increase fluidity (Lieleg et al., 2008). *In vivo*, mice with mutations in NM-II-A or NM-II-B have heart defects and hydrocephalous, respectively, and are embryonically lethal (Tullio et al., 1997; Conti et al., 2004). In contrast, NM-II-C mice survive to adulthood and are viable (Ma et al., 2010). These data suggest that the cytoskeleton, cross-linked by myosin motors, may be contributing to the shape changes in cells that are necessary for embryonic development.

1.2 DEVELOPMENT OF THE MOUSE INNER EAR

The mouse inner ear is an excellent model system by which to further understand the impact of cell mechanics on cell structure and tissue function. The structure of the inner ear (Slepecky, 1996) can be sub-divided functionally into the auditory and vestibular epithelia. The auditory sensory epithelium, the cochlea, is responsible for hearing function and can be further divided into three domains (Figure 3). The neural domain, which includes spiral ganglion neurons and surrounding non-neuronal mesenchymal and glial cells, sends auditory stimuli to central projections for higher auditory processing. The sensory domain, the organ of Corti, converts sound waves into electrochemical signals that are transmitted to spiral ganglion neurons. Finally, the non-sensory domain contains supporting cells that maintain ionic homeostasis (Kikuchi et al., 2000) and structural integrity of the cochlea. These structures were initially characterized based primarily on cell shape, morphology, and position within this auditory epithelium. However, it is still unclear how these domains are specified and organized within the cochlea.

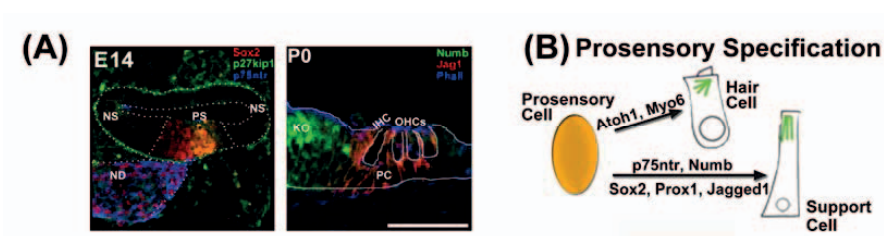

Figure 3. Development of the organ of Corti (OC). (A) The developing cochlear duct at embryonic day 14 (E14) can be sub-divided into three domains, the neural domain (ND), prosensory domain (PS), and non-sensory domain (NS). This apical region of the prosensory domain will give rise to the OC, and is

shown here to express prosensory marker Sox2 (red) and cell cycle regulator $p27^{Kip1}$ (green). The ND also expresses Sox2 and is immunopositive for neurotrophin receptor p75 ($p75^{ntr}$). By postnatal day 0 (P0), both inner hair cells (IHCs) and outer hair cells (OHCs) have Phalloidin (blue) labeled actin stereocilia bundles, and are arranged in stereotyped rows that are separated by non-sensory supporting cells that are shown here to express either Jagged1 (red) in the OC or Numb (green) in Kölliker's organ (KO). **(B)** Prosensory specification is the first stage in the differentiation of the OC. Prosensory cells can be specified into either hair cells, which express hair cell markers Atoh1, and later Myosin6, or support cells, which can express one or several markers of differentiation, including Sox2, Prox1, Jagged1, $p75^{ntr}$, or Numb. Scale bar 50 µm.

The organ of Corti (**Figure 4**) contains two types of mechanosensory hair cells that are distributed into a single row of inner hair cells (IHCs) and three rows of outer hair cells (OHCs). Additionally, there are 7 types of non-sensory supporting cells. Supporting pillar cells (PCs), between IHCs and OHCs, form the fluid-filled tunnel of Corti during postnatal stages of mammalian development. Deiters' cells interdigitate between the three rows of OHCs and also form fluid-filled spaces of Nuel below the OHC lumenal surface. Similarly, inner phalangeal cells are interdigitating the IHC row. Claudius', Hensen's, and Boettcher's cells are located lateral to the OHCs, and form the lateral edge of the organ of Corti. The medial edge of the organ of Corti contains non-sensory cells of the greater epithelial ridge, also known as Kölliker's organ, which will develop into the cells surrounding the fluid-filled inner sulcus. The apical surface of the organ of Corti, herein referred to as the lumenal surface, is covered by the tectorial membrane, while the basolateral surface is bounded by the basilar membrane. The specialized cellular structure and patterning of this epithelium begins during embryonic stages of development and continues through the postnatal period until the onset of hearing at postnatal day 12 (P12) in the mouse (Alford and Ruben, 1963).

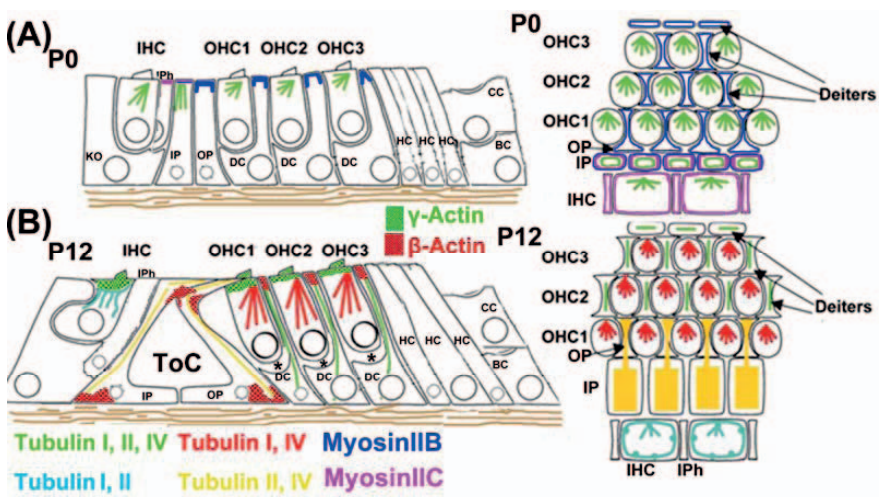

Figure 4. Distribution of cytoskeletal proteins in the organ of Corti (OC). (**A**) Views of the postnatal day 0 (P0) OC in cross-section (left) and whole-mount (right) shows one row of IHCs and three rows of OHCs with interdigitating non-sensory supporting cells, IPh, inner phalangeal cell; IP, inner pillar cell; OP, outer pillar cell; Deiters' cell, DC; HC, Hensen's cell; CC, Claudius' cell; BC, Boettcher's cell. Microtubule isotypes and Myosin II localization are shown in both views. (**B**) Views of the P12 OC in cross-section (left) shows fluid filled spaces including the tunnel of Corti (ToC) and spaces of Nuel (asterisk) as well as the differential distribution of γ- and β-Actin isoforms. Whole-mount view (right) shows differential distribution of microtubule isotypes in hair cells and support cells in the OC. Adapted from Jensen-Smith et al., 2003.

Research on cochlear development has taken advantage of genetic ablations in the mouse to relate transcription factors to the specification (Figure 3) and formation of cochlea-specific hair cells and supporting cells (Kelley et al., 2009). The cochlear duct extends from an invagination of the hindbrain beginning between embryonic day 10 (E10) and E12. By E12, LIM-homeodomain transcription factor Islet1 is expressed within the cochlear duct in cells that will give rise to cells in the prosensory and proneural domains (Radde-Gallwitz et al., 2004). In addition, the sex-determining-region-Y box transcription factor Sox2 is expressed in prosensory cells (Kiernan et al., 2005), proneural cells (Puligilla et al., 2010) and newly differentiated supporting cells in an antagonistic interaction with Atoh1 (Dabdoub et al., 2008). The basic helix-loop-helix transcription factor Atoh1 (Ben-Arie et al., 1996) is expressed in prosensory cells and the time when sensory cell specification begins at E13. A majority of these cells will develop into hair cells (Driver et al., in press), and Atoh1 is essential for hair cell formation (Bermingham et al., 1999). Interestingly, inner-PCs maintain some plasticity during postnatal development, as ectopic expression of Atoh1 in these cells induces expression of hair cell markers (Liu et al., 2012). It is not yet clear why PCs lose the ability to transdifferentiate into hair cells, or how this ability might be extended. Finally, the prospero-homeobox transcription factor, Prox1, is expressed in the developing sensory epithelium in embryonic development and down-regulated in OHCs before birth at E18. Expression is maintained only in a subset of non-sensory supporting cells, PCs and Deiters' cells, only through the first two postnatal weeks (Bermingham-McDonogh et al., 2006). Together, these data help to clarify the mechanisms of cell specification in the sensory domain of the cochlea. However, specification of the prosensory cells that will eventually give rise to hair cells and supporting cells is still not well understood.

It has been suggested that the specification of prosensory cells as either hair cells or supporting cells is the result of lateral inhibition (Gierer and Meinhardt, 1974) organized by mosaicism in expression of ligands and receptors in the Notch signaling pathway (Lewis, 1996). Previous reports have shown that developing hair cells express Notch ligands Delta-like 1 and Jagged2. Genetic deletion of either of these genes or their receptor, Notch1, leads to an increase in the number of hair cells as a result of the loss of lateral inhibition (Lanford et al., 1999; Kiernan et al., 2006). Later, during late embryonic stages of development, Notch ligand Jagged1 is expressed in the cochlea in supporting cells immediately adjacent to hair cells and extends into Kölliker's organ at E17.5 (Morrison et al., 1999). In addition, neurotrophin receptor p75 ($p75^{ntr}$), is also expressed in the cochlea from E14.5 through the early postnatal period (Gestwa et al., 1999). Expression data also show this receptor to be localized to a subset of supporting cells, PCs, and show that down-regulation of this receptor occurs in the first postnatal week of development. Interestingly, $p75^{ntr}$ is dispensable for cochlear development (Brors et al., 2008), but deletion of $p75^{ntr}$ leads to early onset hearing loss (Sato et al., 2006). From these data, it is clear that a better understanding of supporting cell differentiation may increase the potential for therapeutic alterations to support cell plasticity through postnatal stages of development.

In addition to transcriptional specifications, the concomitant regulation of cell number is also an important developmental process in the embryonic organ of Corti. Cell cycle exit begins in apical regions of the organ of Corti at E13 (Ruben, 1967). However, the regulators of cell cycle progression that have been studied extensively in isolated mitotic cells (Mitchison and Salmon, 2001) are still not fully characterized in the cochlear sensory epithelium. Targeted deletion of cell cycle regulator Retinoblastoma protein leads to cell-cycle re-entry and an over-proliferation of cell

within the cochlear sensory epithelium (Sage et al., 2005). Similarly, deletion of cyclin-dependent kinase inhibitor $p27^{Kip1}$, also results in prolonged cellular proliferation, an increase in hair cells and support cells, and deafness (Chen and Segil, 1999) and is largely responsible for cell-cycle control in the organ of Corti (Lee et al., 2006). As both of these cell-cycle regulators maintain their expression in supporting cells longer than hair cells, it may be possible to regulate cell-cycle controls to proliferate hair cells in damaged cochleae.

While hair cell and supporting cell specification occurs in embryonic stages of mouse development, these cells also undergo extended and distinct stages of structural differentiation throughout postnatal development (**Figure 4**). The OHCs develop actin-rich mechanosensory hair bundles, stereocilia, which are stabilized within an actin-dense meshwork called the cuticular plate. The cuticular plate of OHCs contains both β- and γ-actin, and mutations disrupting either isoform lead to early onset age-related hearing loss (Perrin et al., 2010), suggesting that these isoforms each function to maintain OHC structure, but are not necessary for OHC structural development. Furthermore, the development of the cuticular plate is thought to be constrained by the organization of the stereocilia (Etournay et al., 2010). Mutations in γ-actin have also been linked to human deafness loci DFNA20/26 (Zhu et al., 2003; Morín et al., 2009). Myosins, which regulate cytoskeletal motility by cross-linking actin filaments, also impact OHC shape and structural integrity. Several myosin motor proteins have been shown to localize to the cochlea and impact hair cell structure (Coling et al., 1997; Richardson et al., 1997; Belyantseva et al., 2005). For example, Myosin 6 localizes to the cuticular plate of IHCs and OHCs (Avraham et al., 1995) and loss of this protein leads to degeneration of the mouse sensory epithelium by P18 (Avraham et al., 1995). Along the lateral wall of the OHCs, an actin-based spectrin-cross-linked cortical lattice (Holley and Ashmore, 1990) attaches to the plasma membrane by as yet unidentified pillars (Forge, 1991; Fridberger et al., 2009). Measurements of the distance between filaments in this lattice suggest that the cortical actin primarily contributes to the circumferential stiffness and shape of the OHC (Holley et al., 1992). Stiffness measurements in isolated adult OHCs suggest that the plasma membrane also contributes to the mechanical properties of the cortical actin network (Tolomeo et al., 1997). However, the actin-dense cuticular plate stiffness has not yet been measured.

In contrast to OHCs, mature PCs are composed primarily of 15-protofilament microtubules. Polymerization of microtubules is thought to proceed during early postnatal development from the lumenal surface, down the longitudinal axis of the cell towards the basolateral surface in contact with the basilar membrane (Hallworth et al., 2000). There are several types of post-translational modifications of microtubules, including acetylation, tyrosination, detyrosination, and polyglutamylation. It is known that microtubules with low turnover and high stability have more modifications (Wloga and Gaertig, 2010), but it is unclear whether these modifications are a consequence or a cause of microtubule dynamics. PC microtubules are first acetylated and then detyrosinated during postnatal development (Tannenbaum and Slepecky, 1997). These post-translational modifications suggest that PCs contain stable microtubules relative to OHCs, which are primarily composed of tyrosinated microtubules (Slepecky et al., 1995). PCs also contain a network of actin filaments localized to the apical surface and footplate contacting the basilar membrane. Relative to OHCs, PCs contain more γ-actin and less β-actin at the apical surface, and a differential distribution of actin isoforms is present between apical and basal PCs (Furness et al., 2005). Actin and microtubules are further stabilized within the cytoplasm by the presence of tropomyosin (Slepecky and Chamberlain, 1987) and myosin II (Yamamoto et al., 2009). Together, these data

suggest that many of the cytoskeletal components described here (Fig. 1), may have a functional role dictating cell structure and cell mechanical properties during development.

The structural development and patterning of the cochlear sensory epithelium are essential for hearing function. In the cochlea, sounds are spatially arranged by frequency domains. Even complex sounds are mapped by frequency onto the cochlea and these sounds vibrate discrete regions of the basilar membrane. Each area of the basilar membrane shows maximal response to one frequency. The base of the basilar membrane responds maximally to high frequencies and the apex responds to low frequencies. This graded response along the longitudinal direction of the basilar membrane is referred to as a tonotopic gradient (von Békésy, 1956). In order to achieve this resolution of different frequencies along different locations, the properties of the basilar membrane also show some gradients in morphology. The basilar membrane is thin and narrow at the base, and wide and thick at the apex (Kimura, 1975; Dallos, 1996). However, measurements of point stiffness made in the radial direction, from medial PCs laterally to the OHC rows, on the basilar membrane also show a gradient in response (Olson and Mountain, 1994; Emadi et al., 2004). This suggests the observed difference in stiffness at different radial locations of the basilar membrane may have a cellular basis. It is clear that these sensory and supporting cells are required for hearing function. At a cellular level, hearing loss is observed in animal models that exhibit a misdirected development of patterning in the epithelium, or a collapse of fluid-filled spaces, such as the inner sulcus (Rüsch et al., 2001), spaces of Nuel (Merchant et al., 2004) or tunnel of Corti (Colvin et al., 1996; Hayashi et al., 2007; Puligilla et al., 2007). It is thought that the PCs that form the tunnel of Corti provide structural support to the organ of Corti, and stiffness measurements on isolated adult PCs suggest that microtubules contribute most to the cell mechanical properties (Tolomeo and Holley, 1997). Therefore, it is of great interest to measure the mechanical properties of these cells within the organ of Corti, and modulate either hair cell and supporting cell specific markers, or cytoskeletal components, to determine the impact of cell development on hearing function.

1.3 FIBROBLAST GROWTH FACTORS IN COCHLEAR DEVELOPMENT

The growth, proliferation and differentiation of the cells required for the formation of the organ of Corti is mediated through growth factor signaling. One important subset of growth factor signaling is the Fibroblast growth factor (Fgf) signaling pathway. Secreted Fgfs bind to a subset of tyrosine kinase Fgf-receptors (Fgfrs). This sub-family contains Fgf ligands that can bind to Fgf-receptors (Fgfrs), which signal intracellularly by activating tyrosine kinases. The Fgf-family contains 23 ligands and 7 different Fgfr proteins, which vary in ligand binding affinity (Olsen et al., 2004), dimerization (Mangasarian et al., 1997) and affinity for heparin sulfate proteoglycans (Ibrahimi et al., 2004). The latter are necessary for receptor binding to an Fgf ligand (Shimokawa et al., 2011). Fgfrs can be further sub-divided by the mechanism of action, as some can signal over short, paracrine, or long, endocrine-like distances (Ornitz, 2000).

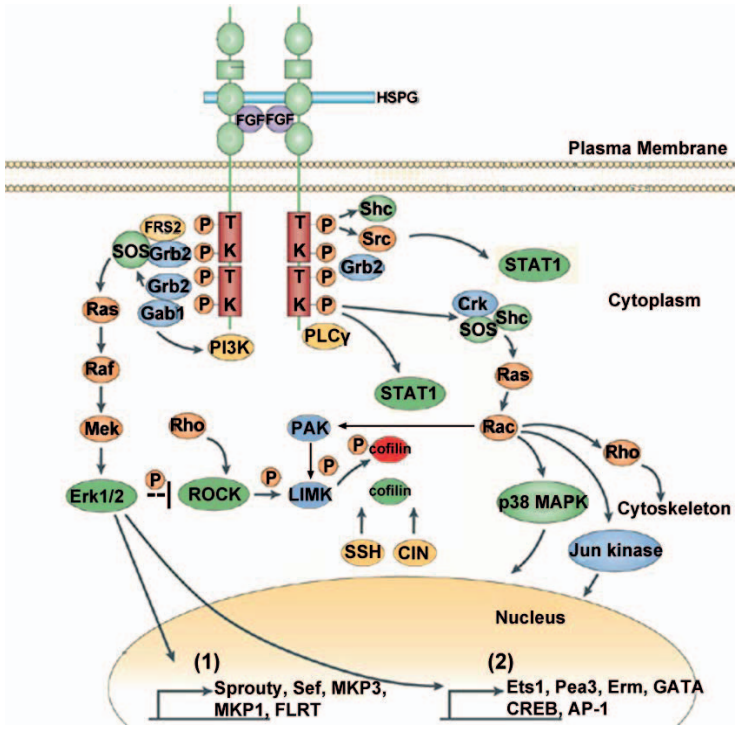

Figure 5. Downstream activation of Fibroblast growth factor (Fgf) signaling pathway. As shown, Fgf ligands bind in the presence of HSPG, heparin sulfate proteoglycan, to Fgf-receptors that can affect several downstream cascades including MAPK, PLC-γ, PI3K, and STAT to control growth, proliferation, and differentiation of the cell. Transcriptional targets have been divided into those that feedback on Fgf-signaling **(1)**, and transcription factors **(2)**. P, phosphate; Shc, Src homology 2 domain-containing protein; Src, non-receptor tyrosine kinases; Grb2, growth factor receptor bound protein-2; Frs2, Fibroblast growth factor receptor substrate 2; SOS, guanine nucleotide exchange factor Son of Sevenless; Crk, adaptor molecule binding to tyrosine-phosphorylated proteins; Ras, Rat sarcoma small GTPase protein; Rac, small Rho GTPase family member; PAK, serine/threonine-protein kinase; LIMK, Lim-domain-kinase; SSH, slingshot; CIN, chronophin, cofilin-activating phosphatase; Erk1/2, extracellular signal-regulated kinase; p38 MAPK, mitogen-activated kinase; T.K., Tyrosine Kinase. Adapted from Mason, 2007 and Bernstein and Bamburg, 2010.

Receptor dimerization leads to activation of four key pathways (**Figure 5**): MAPK, PI3K, STAT, and PLC-γ (Itoh and Ornitz, 2011). Fgf-induced MAPK activation occurs in the developing zebrafish telencephalon (Shinya et al., 2001), embryonic chick (Stavridis et al., 2007), and vertebrate limb bud (Gros et al., 2010). These data suggest that MAPK activation is essential for the growth and differentiation of target tissues, including the cochlea. In adult stages, the cochlea upregulates MAPK signaling in response to noise trauma (Jamesdaniel et al., 2011), and has been observed in the presence of hair cell death (Matsui et al., 2004; Lahne and Gale, 2008). The role of MAPK signaling in cochlear development has not yet been fully described. However, studies in the avian auditory epithelium, which maintains the potential to regenerate, have shown that MAPK inhibition decreases supporting cell proliferation during regeneration (Witte et al., 2001; Bell and Oberholtzer, 2010). The specificity of Fgf-signaling through different downstream cascades is thought to be regulated by the presence and binding of adaptors and co-factors such as Fgfr-specific substrates, Frs molecules (Hoch and Soriano, 2006) and growth-factor receptor bound protein Grb2 (Lin et al., 2012). Like many growth factor signaling cascades, Fgf-induced MAPK

signaling has been shown to be associated with regulatory feedback loops. In particular, activation of transcription of *MKP3* leads to production of a MAPK-phosphatase that negatively regulates Fgf-signaling (Li et al., 2007).

Fgf ligands can bind multiple Fgf receptors (Olsen et al., 2004). Many of these ligands are transcribed from genes that either map to deafness loci or are associated with congenital deafness (Fgfs 1, 3, 6, 8, 13, 14, 20, 22). One-third of these 23 ligands have very low or no expression in the cochlea (Fgfs 2, 4, 6, 11, 15, 17, 22, 23). All four genes that encode Fgfr proteins are expressed in the developing cochlear duct (Pickles, 2001; Hayashi et al., 2010). *Fgfr4* mRNA expression localizes this receptor to the mesenchyme surrounding the sensory epithelium. *Fgfr1* is expressed on the medial side of the cochlear duct in presumptive OHCs and the greater epithelial ridge cells as early as E13.5. This receptor has been implicated in patterning of the sensory epithelium during embryonic development (Pirvola et al., 2002). *Fgfr2* is expressed on the lateral side of the cochlear duct in non-sensory supporting cells of the spiral ligament and in Hensen's and Claudius' cells. This receptor is thought to have a paracrine mode of action in the developing cochlear duct (Privola et al., 2000). Furthermore, this gene has been mapped to a known deafness locus, DFNB57, and is associated with several types of craniosynostosis (Orvidas et al., 1999; Desai et al., 2010).

Fgfr3 is not expressed in early embryonic development, but is present in the late embryonic period (E16.5-E18) broadly within the sensory epithelium in both hair cells and supporting cells. However, by postnatal day 0, *Fgfr3* mRNA expression is down-regulated in OHCs and persists in non-sensory pillar and Deiters' cells (Mueller et al., 2002; Hayashi et al., 2010). Mutations in Fgfr3 lead to achondroplasia and deafness in both humans (Doherty et al., 2007) and mice (Colvin et al., 1996; Hayashi et al., 2007; Puligilla et al., 2007). One hallmark of this mutation in the cochlea is the malformation of the pillar cells that mature to form the Tunnel of Corti. This suggests that Fgf-signaling plays a role in pillar cell structural development. However, it remains to be seen how Fgf-signaling exerts control over cytoskeletal formation.

1.4 THYROID HORMONE SIGNALING

Another important growth factor for cochlear development is thyroid hormone. Thyroid hormones are tyrosine-based hormones produced in the thyroid gland. Circulating thyroid hormone, thyroxine (T4), which takes advantage of a long half-life (Brown-Grant, 1967), travels through the blood stream to target tissues (**Figure 6**). This inactive T4 is converted into the active form, triiodothyronine (T3), by iodothyronine deiodinase selenoenzymes through a de-iodination reaction. If there is a deficiency of iodine, then this mineral could be the limiting reagent in the production of active T3. There are three known de-iodinase enzymes (Galton, 2005). Deiodinase 1 (D1) and D2 can convert T4 into T3. However, there are data to suggest that these two enzymes are not functionally redundant, as D1 is dispensable for mammalian development (Schneider et al., 2005) while inactivation of D2 leads to decreased regulation of thermogenesis in brown adipose tissue (de Jesus et al., 2001). Overall, these $D2^{-/-}$ mice have a phenotype consistent with pituitary resistance to T4 (Schneider et al., 2001). D3 is known to convert the high affinity T3 ligand, and T4, into a functionally inactive thyroid hormone, rT3 (Galton, 2005), which suggests that this enzyme negatively regulates thyroid hormone signaling in most target tissues. In the cochlea, *D2* is present in the cochlear duct within the first postnatal week of development and localizes to non-sensory domains that include spiral ligament and osseous spiral lamina (Ng et al., 2009). $D2^{-/-}$ mice show a developmental delay in cochlear development and 40dB

auditory brainstem response threshold shift (Ng et al., 2004). In contrast to D2, *D3* is expressed in late embryonic stages of development, and localizes to non-sensory domains including stria vascularis, spiral ganglia, and tympanic border cells beneath the basilar membrane (Ng et al., 2009). *D3*$^{-/-}$ mice show acceleration of cochlear differentiation and 70 dB sound pressure level hearing loss (Ng et al., 2009).

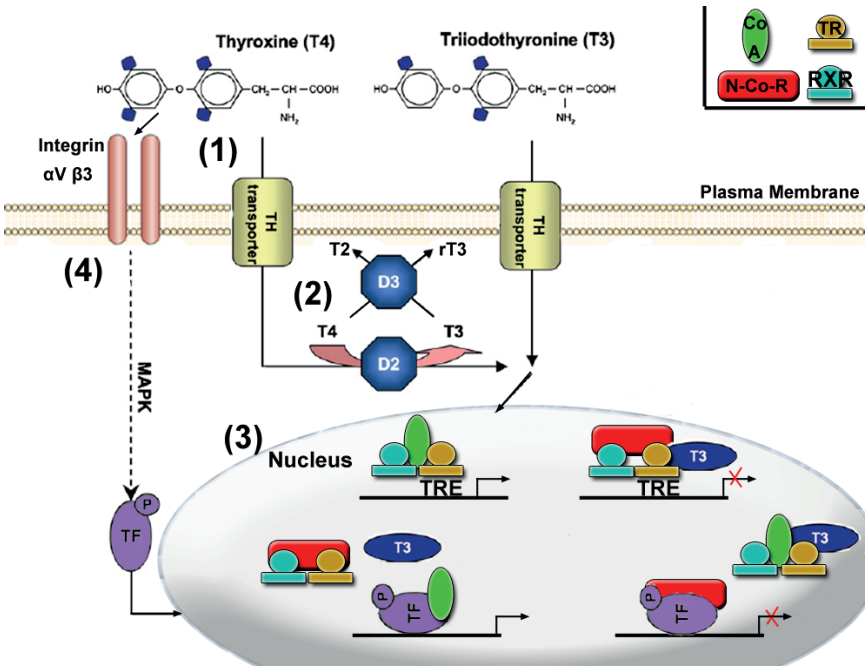

Figure 6. Thyroid hormone action. Schematic representation of some mechanisms by which thyroid hormones (T3 and T4) regulate gene transcription. (**1**) Circulating T3/T4 enter target tissues via thyroid hormone transporters, including Lat1, Mct8&10, and Oatp1c1. (**2**) Inside the cytoplasm, T3 levels are tightly controlled by the activity of deiodinase selenoenzymes (D2/D3). (**3**) Inside the nucleus, T3 bound to thyroid hormone receptors (TRs), which can heterodimerize to Retinoid X Receptor (RXR), can activate or repress gene transcription through binding with co-activators or nuclear-co-repressors (N-Co-Rs). (**4**) Alternatively, T4 can bind to Integrin receptors, which then activate transcription factors (TF) capable of regulating target gene transcription in the nucleus. Figure adapted from Weitzel, 2008, and Horn and Heuer, 2010.

More recently, research efforts have focused on the mechanisms used by target tissues to carry circulating T4 into target cells. These thyroid hormone transporters are well-characterized in several target tissues including the monocarboxylate transporters (Mcts) in the central nervous system (Schweizer and Köhrle, 2012). However, thyroid hormone transport in the cochlea is not well understood. First characterization of thyroid hormone transporters noticed much overlap between transporters Lat1, Mct8, Mct10, Oatp1c1, and deiodinase enzymes (Sharlin et al., 2011), particularly in the greater epithelial ridge, tympanic border cells, and spiral ligament. During development *in utero*, the availability of thyroid hormones is based solely on maternal production (Patel et al., 2011) and thyroid hormone transport across the placenta is sensitive to iodine uptake (Burns et al., 2011), as well as thyroid hormone binding proteins (McKinnon et al., 2005; Mortimer et al., 2012) and transporters (Loubière et al., 2010). Together, these data suggest multiple layers of potential regulatory mechanisms on thyroid hormone metabolism during development.

Two thyroid hormone receptor (TR) genes, *Thra* and *Thrb*, are post-transcriptionally modified to encode the 4 nuclear receptors—*Thra* encodes TRα1 and TRα2, while *Thrb* encodes TRβ1 and TRβ2. In the cochlea, expression of *Thrb* is evident as early as E12.5 (Bradley et al., 1994). By P1, *Thrb* expression is down-regulated in the sensory epithelium and refined to a subset of cells within the greater epithelial ridge (Ng et al., 2009). In contrast, *Thra* expression is evident by P0 in the spiral ganglia of the cochlear and vestibular organs. These expression patterns are particularly interesting given the late onset of expression of deiodinase enzymes (Ng et al., 2009) and suggest a potential ligand-independent action by TRs. Loss of TRβ1 impairs auditory function by disrupting potassium currents in IHCs (Forrest et al., 1996), showing this receptor to be necessary for hearing function. In contrast, loss of TRα1 leads to abnormally slower heart rate and decreased body temperature in mice (Wikström et al., 1998). Mutations causing deletion of all known thyroid hormone receptors delay differentiation of the organ of Corti and result in malformations of the tectorial membrane, inner sulcus, and tunnel of Corti (Rüsch et al., 2001), which suggests that there are some receptor-independent or compensatory mechanisms of thyroid hormone signaling on cochlear structural development.

Thyroid hormone action (**Figure 6**) through TRs can result from homodimerization (Piedrafita et al., 1995) or heterodimerization with Retinoid X Receptors (RXRs) (Yu et al., 1991; Kliewer et al., 1992). It was shown that heterodimerization stabilizes TRs on DNA (Hallenbeck et al, 1992) but it is still not clear the extent to which receptor binding is a transient or sustained phenomenon. In either case, the mechanism for this stability was further examined with X-ray crystal structures of the ligand-binding domain, which suggest that this region mediates the probability of TRs to interact as homodimers or heterodimers with RXRs (Ribeiro et al., 2001). TRs can regulate target gene transcription through binding to thyroid hormone response elements (TREs) (Desvergne, 1994) in promoter or enhancer regions. There is also evidence of non-classical activation by TREs within introns (Sap et al., 1990). The TRE consensus sequence, 5'-AGGTCA-3' (Umesono et al., 1991) usually appears as tandem repeats, which can be direct repeats, inverted, or everted. Direct repeats are occupied by homodimers (Umesono et al., 1991). An inverted repeat, or palindromic sequence, has been characterized in the promoter region of growth hormone (Glass et al., 1987) and the everted repeat has been shown to have the potential for ligand-independent activation (Sjöberg and Vennström , 1995). It was first shown that the spacing of these and other consensus sequences was the primary factor that directed binding of homodimers or heterodimers to DNA (Forman et al., 1992), but it is also possible that the presence of ligand and the aforementioned dimerization can impact TR binding to DNA. Finally, a synthetic receptor was engineered to show that it is possible for TRs to bind monomer TREs (Katz and Koenig, 1994), but a thyroid hormone target gene containing a monomeric site in the promoter region has yet to be identified.

Thyroid hormone receptors can act as either activators or repressors of target gene transcription. This additional layer of regulation on TRs has been attributed to the specificity of thyroid hormone associated proteins (Koenig et al., 1998). These proteins are sub-divided into transcriptional co-activators or co-repressors. Co-activators of nuclear receptors, including TRs, recognize a signature amino acid motif, LXXLL (Heery et al., 1997), where L is leucine and X is any other amino acid. However, some co-activators, such as the protein Trip230 can vary in binding as a result of conformational changes in the TR ligand-binding domain (Chang et al., 1997). Co-repressors also play an important role for TRs bound to DNA independent of ligand. These proteins bind a hinge region between the ligand and DNA binding domains of

TRs (Hörlein et al., 1995) and include the family of nuclear-co-repressors N-CoRs, (Hörlein et al., 1995) and silencing mediator of retinoid and thyroid receptors, SMRTs (Chen and Evans, 1995). The mechanism of T3-dependent repression of gene transcription remains poorly understood relative to the mechanisms of co-activators, in part as a result of a lack of similar co-repressor activity in the model yeast *S. cerevisiae* (Olson et al., 1998). Taken together these data support a further need for understanding the mechanisms of thyroid hormone and TR action, and the complex interactions between multiple signaling networks.

There is a growing body of evidence to support the hypothesis that there may be cross-talk between thyroid hormone and Fgf-signaling pathways. For example, overproduction of thyroid hormone will induce negative feedback mechanisms (Kaplan and Yaskoski, 1982) to prevent an overload of T3 in the central nervous system. However, treatment with Fgf ligand also induces a concentration dependent increase in D3 activity (Esfandiari et al., 1992). This regulation can vary by tissue type. Fgf also increases expression of D2 protein in cultured astrocytes (Lennon et al., 1994) that was sustained over 24 hours *in vitro*. It is unclear whether these pathways have a mutual dependency on target genes that induce feedback mechanisms directly, or if Fgf-signaling indirectly regulates thyroid hormone status. In contrast to the regulation on thyroid hormone by Fgf, it is clear that thyroid hormones have a direct impact on the Fgf-signaling pathway. First, T3 stimulates expression of all Fgfr's (Barnard et al., 2005). Second, a thyroid hormone response element is present in the promoter region of *Fgfr1* (O'Shea et al., 2007). Finally, thyroid hormone regulates heparin sulfate expression in the developing growth plate. Images from tibial growth plates of the mouse show increased proteoglycan expression when low levels of T3 are present (Bassett et al., 2006). Together, these data suggest multiple stages of regulation by thyroid hormones on Fgf-signaling, and motivate a further understanding of thyroid hormone action specifically in the cochlea.

1.5 SPECIFIC AIMS

The development of the cochlea impacts auditory function. Cochlear hair cell and support cell development is regulated by the timing of differentiation and cytoskeletal formation. However, the impact of the developing cytoskeleton on cell mechanics has not been quantified. The first aim of this thesis is to measure the surface mechanical properties of developing OHCs and PCs, in the intact sensory epithelium using AFM, and characterize the impact of cytoskeletal structure on developing cell mechanics. Since cytoskeletal formation is often the result of growth factor stimulation, the second aim of this thesis is to assess the impact of Fgf and thyroid hormone signaling upstream of cytoskeletal growth and cell mechanical properties. Finally, the specification of prosensory cells within the organ of Corti may lead to early detection of different mechanical properties of sensory hair cells and non-sensory supporting cells. Therefore, the third aim of this thesis seeks to characterize the convergence of multiple markers of differentiation in order to define the prosensory region in the organ of Corti before hair cell and support cell specification.

2 MATERIALS AND METHODS

2.1 COCHLEAR EXPLANT CULTURES

Cochleae from Institute for Cancer Research (ICR) mice (Charles River Laboratories, Frederick, Maryland, USA) were cultured at specific stages between E16 and P5 as previously described (Montcouquiol and Kelley, 2003). Briefly, the temporal bone was harvested from a hemi-sectioned mouse skull, and the cochlear sensory epithelium was exposed by removing the bony capsule, stria, Reissner's membrane, and tectorial membrane. All dissections were performed in 1X Hanks Buffered Salt Solution (Invitrogen, Frederick, Maryland, USA) containing 1mM (4-(2-hydroxyethyl)-1-piperazineethanesulfonic acid) (HEPES) (Invitrogen) and brought to pH 7.4 with 10N NaOH (Fluka, Sigma-Aldrich, Reston, Virginia, USA). Cochleae were plated on 3% Matrigel (BD Biosciences, Bedford, Massachusetts, USA) -coated No.1 glass coverslips (Corning, New York, USA) and cultured in 200 µL Dulbecco's Modified Eagle Medium, DMEM (Invitrogen), containing 0.1 mg/mL Ciproflaxin HCl (Mediatech Inc., Corning, New York, USA) and 1X N2 supplement (Invitrogen). Cochlear explant cultures varied in thickness from 30-50 µm. Fgfr3-deficient mice were kindly provided by Dr. David Ornitz (Washington University in St. Louis, Missouri, USA). These and Atoh1$^{lacZ/+}$ reporter mice were bred on a C57 black 6 background strain (Charles River Laboratories, Frederick, Maryland, USA) to generate Atoh1$^{lacZ/+}$ or *Fgfr3*$^{-/-}$ animals. *Fgfr3*$^{-/-}$ mice are viable but have a 60 dB sound pressure level hearing loss compared to wild-type littermates (Colvin et al., 1996). Additionally, cochleae from Deiodinase 2 knockout mice (D2$^{-/-}$), which have a phenotype consistent with hypothyroidism in the cochlea (Ng et al., 2004), and littermate controls were kindly provided by the laboratory of Dr. Douglas Forrest (NIDDK, Bethesda, Maryland, USA). All animal care and procedures were approved by the Animal Care and Use Committee at NIH and complied with the NIH guidelines for the care and use of animals.

2.1.1 Pharmacology

To decrease thyroid hormone signaling *in vivo*, animals were treated with 0.02% methimazole (Sigma) and 10% sucrose (MP Biomedicals, Solon, Ohio, USA,) in drinking water and low iodine feed (TD.120363, Harlan Laboratories, Madison, Wisconsin, USA) administered *ad libitum*. To increase thyroid hormone signaling *in vitro*, explants were treated with 5 µM triiodothyronine (Sigma-Aldrich) or 5 µM reverse triiodothyronine (Sigma-Aldrich), an inactive form of thyroid hormone, as a control, in DMSO. To disrupt the cytoskeleton *in vitro,* tissue cultures were treated after 12-17 hours *in vitro* for 30 minutes with one of the following: 1 µM Latrunculin A (Sigma-Aldrich) in DMSO, 5 µM Jasplakinolide (Sigma-Aldrich) in DMSO, 10 µM Blebbistatin (Sigma-Aldrich) in DMSO, 1 µM Taxol (Sigma-Aldrich) in DMSO, 5 µM Nocodazole (Sigma-Aldrich) in 1X PBS, or vehicle control added to Leibovitz's media (GIBCO, Invitrogen). To affect the Fgf signaling pathway, tissue explants were treated immediately after plating with either 10 µM SU5402 (EMD Chemicals, Millipore, Billeria, Massachusetts, USA) in DMSO, or 1 µM Fgf2 (R&D Systems, Minneapolis, Minnesota, USA) in 1X PBS with 0.1% DMSO and 1 µg/ml heparin sulfate alone or in combination with one of the following: 5 µM Y27632 (Sigma-Aldrich) in sterile water, 10 µM SP600125 (Sigma-Aldrich) in DMSO, or 1 µM U0126 (Sigma-Aldrich) in DMSO.

2.2 OUTER HAIR CELL (OHC) VOLTAGE-DEPENDENT CAPACITANCE

Organ of Corti explants were dissected at postnatal day P4 and cultured in DMEM supplemented with 25 mM HEPES, 7% fetal bovine serum (Invitrogen) and 10 µg/ml ampicillin (Calbiochem, Millipore) at 37°C and 5% CO_2 as described previously (Russell et al., 1986; Russell and Richardson, 1987; Stepanyan et al., 2006). The organ of Corti explants were cultured 2 to 6 days *in vitro*. Experiments were performed in L-15 cell culture media (Invitrogen) containing the following inorganic salts (in mM): NaCl (137), KCl (5.4), $CaCl_2$ (1.26), $MgCl_2$ (1.0), Na_2HPO_4 (1.0), KH_2PO_4 (0.44), $MgSO_4$ (0.81). Hair cells were observed with an inverted microscope (Eclipse TE2000-U, Nikon) using a 100X 1.3 NA oil-immersion objective with differential interference contrast. To access the basolateral plasma membrane of OHCs, the outermost cells were removed by gentle suction with a ~5 µm micropipette. Pipettes for whole-cell patch-clamp recordings were filled with intracellular solution containing (in mM): CsCl (140), $MgCl_2$ (2.5), Na_2ATP (2.5), EGTA (1.0), HEPES (5). Osmolarity and pH of the intrapipette solution were adjusted with D-glucose and CsOH to match corresponding values of the bath (325 mOsm, pH ~ 7.35). The pipette resistance was typically 2–4 MOhm when measured in the bath. Patch clamp recordings were performed with a computer-controlled amplifier (MultiClamp 700B, Molecular Devices). Measurements of cell capacitance were performed using the "membrane test" feature of the pCLAMP 9.2 acquisition software (Molecular Devices), which continuously delivered a test square wave of period of 4 msec to the cell through the patch-clamp amplifier. The errors of the capacitance measurement algorithm of pCLAMP were corrected offline to account for a non-ideal ratio of the access resistance to the membrane resistance as previously described (Frolenkov et al., 2000). To determine the voltage dependence of OHC capacitance, we applied triangular voltage ramps. Measurements of the cell capacitance during test ramps were corrected for the voltage drop along the access resistance of the pipette. Data were fit to the derivative of the Boltzmann function, $C_m(V) = C_0 + Q_{max}\frac{ze}{kT}\frac{b}{(1+b)^2}$, where $b = exp\left(\frac{-ze(V-V_p)}{kT}\right)$, C_0 is the voltage-independent (linear) capacitance, Q_{max} is the electrical charge transferred across the plasma membrane upon transition of the cell from fully extended to fully contracted state, V_p is the potential at the peak of $C_m(V)$, z is the effective valence of a charge moving from the inner to the outer aspect of the plasma membrane, k is Boltzmann's constant, T is absolute temperature (293 Kelvin), and e is the electron charge. To compare the data obtained from different cells, the voltage-dependent (non-linear) capacitance component was divided by the surface area of the plasma membrane with the formula $X_m(V) = \frac{C_m(V)-C_0}{C_0/X_{lb}}$; where $X_m(V)$ is the specific non-linear voltage-dependent capacitance of the plasma membrane in µF/cm^2 and X_{lb} = 1 µF/cm^2 is the specific capacitance of a lipid bilayer.

2.3 ATOMIC FORCE MICROSCOPY (AFM)

Experiments were performed using a commercially available Bioscope II and Bioscope Catalyst AFM (Bruker, Santa Barbara, California, USA) head mounted onto a Zeiss Axiovert 200 inverted microscope and controlled via a Nanoscope V controller (Bruker). Pyramidal shaped, gold-coated, silicon nitride cantilever probes with 0.03 N/m spring constant (part MLCT, Bruker) were used for all measurements. The AFM system and microscope were mounted on a vibrationally isolated table with pneumatic support. To detect the position of the cantilever, a 3.9 mW laser with wavelength 850 nm was focused with a lens, and reflected from a mirror onto the cantilever. At the

beginning of each experiment, the laser was aligned with the cantilever and photodiode detector. Cells were identified after being loaded with 500 nM Calcein AM vital dye (Invitrogen) in Leibovitz's medium (Invitrogen) for 30 minutes and rinsed with fresh Leibovitz's medium. Instrument control to move the sample surface in X and Y dimensions, to move the cantilever in the Z dimension, and data acquisition was performed with commercial Nanoscope software (Bruker). The position of the sample and the cantilever were detected with 10X (Plan Neofluar®, ∞ 0.17, NA 0.30, WD= 5.5 mm, ZEISS) and 40X (Plan Neofluar®, ∞ 0.17, NA 0.75 WD= 0.71 mm, ZEISS) objectives. Contact mode AFM was applied to all samples in 300-500 µL of Leibovitz's medium at 1.5 µm maximum indentation using 3 µm ramps at 1 Hz continuous force ramping to collect 3 force-distance curves for the center of each identified hair cell or supporting cell. For line-scan measurements, a 50 μm^2 region of interest was selected and points over the lumenal surface of the second row of OHCs and PC rows were examined with 2 µm equal spacing. Because the base of IHCs is rotated in explant cultures, these measurements were excluded from the analysis. Relative force-distance curves were collected with ~300 nm trigger threshold using 3 µm force ramping at 1 Hz for three cycles. Images of all samples were collected before, during, and at the conclusion of each experiment using a standard fluorescence lamp (X-CITE 120, Lumen Dynamics Group Inc., Mississauga, Ontario, Canada) and cooled charge-coupled device (Orca R^2, Hamamatsu Photonics K.K., Japan) controlled by AFM acquisition software (Bruker).

2.3.1 Data Analyses

All force-distance curves were processed offline with custom analysis software in MATLAB (Mathworks, Natick, Massachusetts, USA) and fit to the Sneddon model (Sneddon, 1965) to measure Young's modulus (Ym), which is a material property of the cellular resistance to deformation and was calculated with the formula $F = (2/\pi \tan\alpha)(E/(1-\nu^2))\delta^2$; where F is applied force, ν is Poisson's ratio and assumed to be 0.5, δ is cantilever indentation, and α is cantilever tip angle. Only force-distance curves with a goodness of fit (r^2) greater than 0.98 were used. Average Ym (mean±s.e.m.) was calculated from the average of sample measurements of 10 cells within a given region of interest such as the base or the apex of the cochlea.

2.3.2 Statistical Analyses

To test for a normal distribution of the collected data, a Shapiro-Wilk test was performed using MATLAB (Mathworks) software and the formula $W = (\sum_{i=1}^{n} a_i x_{(i)})^2 / \sum_{i=1}^{n} (x_i - \bar{x})^2$, where $x_{(i)}$ is the order statistic, $\bar{x}$ is the sample mean, and a_i are the constants from the covariance matrix of expected values of the order statistic, if the data were from independent and identically distributed random values. To quantitatively describe different distributions in the data, a two-tailed Kolmolgorov-Smirnov distribution difference test was performed using MATLAB software and the formula $D_n = \sup_x |F_n(x) - G(x)|$ where $F_n(x)$ is the experimental cumulative distribution function, $G(x)$ is a standard normal cumulative distribution function, and $\sup_x$ is the supremum, or least upper bound, of distances in the set of data. Means were compared using a custom Excel (Microsoft) spreadsheet and the formula for Welch's T-test $t = \frac{\overline{X_1} - \overline{X_2}}{\sqrt{(\frac{s_1^2}{N_1} + \frac{s_2^2}{N_2})}}$ (Welch, 1947), or the Student's T-test $t = \frac{\overline{X_1} - \overline{X_2}}{s_{X_1 X_2} \cdot \sqrt{\frac{2}{N}}}$ where $\bar{x}$ is the sample mean, s is the sample standard deviation, $s_{X_1 X_2}$ is the pooled

standard deviation, and N is the sample size. The degrees of freedom for Welch's T-test were calculated with a custom Excel spreadsheet and the formula

$$d.f. = \frac{(\frac{s_1^2}{N_1} + \frac{s_2^2}{N_2})^2}{\frac{(\frac{s_1^2}{N_1})^2}{(N_1-1)} + \frac{(\frac{s_2^2}{N_2})^2}{(N_2-1)}}$$

. The degrees of freedom for the Student's T-test were calculated as $2N - 2$. All p-values were corrected with the Bonferroni correction for multiple testing.

2.4 POLYMERASE CHAIN REACTION (PCR)

All genotypes were examined with PCR, which confirmed that the genetic deletion leads to a loss of both ligand binding and transmembrane domains of Fgfr3 (Colvin et al., 1996). Genomic DNA was extracted from animal tail-clips using Easy-DNA™ Kit (Invitrogen). Template DNA was added to illustra© PuRe Taq Ready-to-go© PCR beads (GE Healthcare), and 50 pg custom primers (Invitrogen), and brought to a final volume of 25 µL with PCR grade water (Quality Biological, Gaithersburg, Maryland, USA). 40 cycles of PCR amplification were performed with the following cycling conditions: 94˚C, 30 seconds; 56˚C, 30 seconds; 72˚C, 30 seconds. PCR products were examined with electrophoresis on pre-cast 4% agarose gels (Invitrogen) and compared to molecular weight standards. Primer sequences used were as follows:
Fgfr3 WT, Forward 3'-AGGTATAGTTGACACCATCGGAGGG -5';
Fgfr3 MUT, Forward 3'- TGCTAAAGCGCATGCTGGAGACTGC-5';
Fgfr3 Common, Reverse 3'-GGGCTGGTTATTGGACTCGC -5'.

2.4.1 Quantitative Polymerase Chain Reaction (QPCR)

Cochleae were removed from the temporal bone, and the surrounding mesenchyme, scala vestibuli and scala tympani were removed. 6-8 cochleae were pooled and total RNA was isolated using RNAqueous (Ambion, Grand Island, New York, USA) reagents. Complementary DNA (cDNA) was synthesized from 500 ng total RNA for each condition using a Superscript III first strand synthesis kit (Invitrogen). Amplification was performed with SYBR Green (Applied Biosystems, Foster City, California, USA) and combined with RNAse-free water to a final reaction volume of 10 µL. For RT2 Profiler PCR Array of mouse cytoskeletal regulators (PAMM-088ZA, SABiosciences, Qiagen, Gaithersburg, Maryland, USA), cDNA was combined with RT2 SYBR Green ROX qPCR Mastermix (SABiosciences) and RNAse-free water to a final reaction volume of 25 µL. RT2 Profiler PCR Array experiments were repeated in triplicate for each condition. Amplification of all mRNA was performed on an ABI Prism 7000 (Applied Biosystems) with the following cycling conditions: 40 cycles of 95˚C for 15 seconds, and 60˚C for 1 minute. To calculate fold change, gene expression was normalized to glyceraldehyde 3-phosphate dehydrogenase (GAPDH) and statistical significance was confirmed with student's T-test. Primer sequences used were as follows:
Fgfr1, Forward, 3'-ATGGTTGACCGTTCTGGAAG-5';
Fgfr1, Reverse, 3'-AGAAAAGGGTACGCAGCAGA-5';
Fgfr3, Forward, 3'-GAGACTTGGCTGCCAGAAAC-5';
Fgfr3, Reverse, 3'-GGGCTCACATTTGTGGTCTT-5',
GAPDH, Forward, 3'-ATCCTGTAGGCCAGGTCATG-5';
GAPDH, Reverse, 3'-TATGCCCGAGGACAATAAGG-5'. Six cochleae per condition were pooled for RNA extraction and cDNA synthesis using an RT^2 First Strand Kit (Qiagen). To express similarity among relative cytoskeletal regulator gene expression levels, a hierarchical clustering method was used (RT^2 Profiler™ Software, Qiagen).

This method applied the correlation coefficient as a similarity metric, as well as the absolute expression level and an average linkage method, to calculate the average distances between all pairs of genes.

2.5 IN SITU HYBRIDIZATION

Temporal bones were isolated and fixed in 4% paraformaldehyde (Electron Microscope Sciences) in 1X PBS (Invitrogen) and rinsed for 15 minutes in 1X PBS repeated three times. Six cochleae from each condition were examined at each time point. Samples were passed through a 5-30% sucrose gradient, and embedded in Optimal Cutting Temperature (Tissue-Tek, Electron Microscopy Sciences, Hatfield, Pennsylvania, USA) freezing compound. Samples were stored in air-tight containers at -80˚C before being cryosectioned at 12 µm thickness on a cryostat microtome (CM3050S, Leica). In situ hybridization was performed on 6 sections of each condition with probes specific to Fgfr1 (Gift from Thomas A. Reh) and Fgfr3 (Jacques et al., 2007).

2.5.1 In Situ Hybridization Probes.

Plasmid templates were amplified in GC10 cells grown in Lennox L Base Broth (Invitrogen) containing 50 µg/mL Ampicillin antibiotic (Sigma-Aldrich) for 18-24 hours. Plasmid isolation was performed with a commercially available Maxi Prep kit (Qiagen) and resuspended at approximately 5 µg/µL in buffer TE. Plasmid was linearized for five hours at 37˚C with 20 U/µL restriction enzyme (New England Biolabs, Ipswich, Massachusetts, USA) in 1X restriction buffer (New England Biolabs). Linearization was confirmed with electrophoresis on pre-cast 2% agarose gel (Invitrogen) and compared with molecular weight standards. This DNA template at approximately 1µg/µL was reverse transcribed for two hours at 37˚C to RNA hybridization probe using 20 U/µL RNA polymerase (Roche, Indianapolis, Indiana, USA), 40 U/µL RNAse inhibitor (Roche) and alkaline phosphatase-conjugated digoxigenin (DIG) RNA labeling nucleoside triphosphates (NTPs) at 1X. This RNA probe was concentrated using an ethanol precipitation containing LiCl.

2.5.2 Pre-treatment and Hybridization.

Sections mounted on slides that were stored at -80˚C before use were dried at room temperature before being fixed with 4% paraformaldehyde (Electron Microscopy Sciences) containing 0.2% gluteraldehyde (Electron Microscopy Sciences) in 1X PBS. Slides were rinsed in 1X PBS, bleached in 6% hydrogen peroxide (Fisher Scientific), washed in 0.1% PBS-Tween-20 (PBST), and permeabilized with 20 µg/mL Proteinase K for 2 minutes. This reaction was quenched with 2 mg/mL glycine in PBST for 10 minutes. Finally, the slides were washed in PBST, fixed with 4% paraformaldehyde containing 0.2% gluteraldehyde in 1X PBS, and washed in PBST, before being sealed in Kapak (Minneapolis, Minnesota, USA) pouches containing 10 mL hybridization solution of 50% Formamide (Sigma), 50 µg/mL heparin sulfate, and 50 µg/mL Yeast RNA in 1% Sodium dodecyl sulfate (SDS) set to pH 5 with Sodium-Sodium Citrate (SSC) Buffer. Slides were pre-hybridized for 4-6 hours at 70˚C before RNA probe was added and hybridized overnight.

2.5.3 Post-hybridization wash and Antibody Binding.

The next day, slides containing specimens were removed from Kapak pouches and submerged in 70˚C pre-warmed Formamide containing 1% SDS with gentle agitation. Slides were submerged in 65˚C pre-warmed Formamide containing 2.5% 20X SSC

Buffer with gentle agitation. Slides were washed in 1X Tris-Buffered Saline-0.1%-Tween-20 (TBST) containing Levimasole and blocked with 10% Chicken Serum (Invitrogen) for at least 2 hours at room temperature. Finally, slides were placed in Kapak pouches containing 10 mL of TBST containing Antidioxygenin AP at 1:5000 dilution and incubated at 4˚C overnight on a rocking platform (VWR).

2.5.4 Post-antibody-wash and Detection.

Slides were removed from Kapak pouches and submerged in TBST. Slides were washed in alkaline phosphatase buffer before adding 0.05 g 5-Bromo-4-chloro-3-indolyl-phosphate, NBT (Roche) in 70% dimethyl formamide (Sigma-Aldrich) and 0.03 g BCIP (Roche) in RNAse-free water. This reaction solution was incubated with the specimens until the desired color intensity was reached. All slides treated with the same probe were treated with the same reaction solution for the same duration to compare relative intensities. This reaction was quenched with 1 mM EDTA (VWR Scientific, Reston, Virginia, USA) solution in PBST for 20 minutes at room temperature. Slides were mounted with Fluoromount-G (Southern Biotech, Birmingham, Alabama, USA) mounting solution beneath No. 1 Coverslips (Corning) adhered with commercially available nail polish.

2.5.5 Image Acquisition and Processing

Slides were examined at room temperature using a Nikon Eclipse 800 fluorescence microscope (Melville, New York, USA) in differential interference contrast (DIC) imaging mode with 20X (Plan Apochromat, ∞ 0.17, NA 0.75, WD =1.0 mm, Nikon) and 40X (Plan Apochromat, ∞ 0.14, NA 0.52, WD = 0.14 mm, Nikon) objectives. Images were acquired using a DXM1200 Camera (Nikon) and accompanying camera system software (Nikon). Images were cropped in Adobe Photoshop CS4 (Adobe).

2.6 WESTERN BLOT

Cochlear explants were freshly isolated before total protein extraction. Proteins were extracted from 8-10 cochleae in RIPA buffer containing complete mini protease inhibitor cocktail (Roche), complete phosphatase inhibitor cocktail (Roche), 1 mM Na_3VO_4, and 500 mM NaF. Protein was quantified using the Dc protein assay kit (Bio Rad) and Lowry method with ND-1000 Spectrophotometer (Nanodrop, Wilmington, Deleware, USA). 25 μg total protein per condition was loaded onto 4-12% SDS-PAGE gels (Invitrogen) run for 2 hours at 120 V, transferred to nitrocellulose membrane (Invitrogen), and run for 3 hours at 80 V at 4°C. Membranes were blocked in 0.05% TBST containing BLOTTO (Rockland, Gilbertsville, Pennsylvania, USA) containing 1% Bovine Serum Albumin (Sigma). Primary antibodies were incubated in blocking solution at the following concentrations: p-Fgfr (1:500, Cell Signaling), p-LIMK (1:500, abcam), p-Cofilin (1:500, abcam) Fgfr (1:2500, Life Technologies, Frederick, Maryland, USA), LIMK (1:5000, abcam), Cofilin (1:5000, abcam), and β-Actin (1:5000, Sigma). Primary antibodies were conjugated to horseradish peroxidase anti-rabbit or anti-mouse secondary antibody (1:5000, Amersham) and detected using ECL Detection Reagents (Amersham).

2.6.1 Image Acquisition and Processing

Membranes were visualized using Image Station 4000R (KODAK) and Carestream Molecular Imaging Software (New Haven, Connecticut, USA). Image analysis was performed with ImageJ (Rasband, 1997) using the Gel Analysis plug-in

method to calculate relative density. Relative density of phosphorylated protein signal was normalized to β-actin signal for the same tissue and under the same experimental conditions. Statistical significance was determined with Welch's T-test (Welch, 1947). Images with the median relative density for each antibody in each condition were imported for image preparation by being cropped and resized in Adobe Photoshop CS4 (Adobe).

2.7 TRANSMISSION ELECTRON MICROSCOPY

Cochleae from 3 animals at each time point for each condition were isolated and placed immediately in 0.1 M phosphate buffer (pH 7.4) containing 4% paraformaldehyde and 2% glutaraldehyde for 30 minutes at room temperature followed by 2 hours at 4˚C. The inner ears were then washed in phosphate buffer and cacodylate buffer, post-fixed with 1% osmium tetroxide, dehydrated through a graded alcohol series, and stained with 1% uranyl acetate in 50% ethanol. Samples were embedded in Poly/BED 812 resin (Polysciences Inc., Warrington, Pennsylvania, USA) as previously described (Petralia and Wenthold, 1992). Thin sections of about 75 nm were cut using a Leica Reichert ultramicrotome, stained with lead citrate, mounted on 200-Copper mesh grids (Electron Microscopy Sciences), and examined at room temperature using a JEOL transmission electron microscope (Akishima, Tokyo, Japan) at 80 kV with 15,000X magnification. Images were acquired using a Hamamatsu Camera (Hamamatsu Photonics K.K., Japan) and Advanced Microscopy Techniques Camera System software version 534.4 (Woburn, Massachusetts, USA). Images were formed into composites and cropped in Adobe Photoshop CS4 (Adobe).

2.7.1 Image Quantification

To quantify morphological changes in OHCs and PCs, transverse sections from three animals for each condition were analyzed with ImageJ (Rasband, 1997) analysis software. To quantify the presence of microtubules, a horizontal line was drawn at distances 2, 4, and 6 μm from the lumenal surface of PCs and the number of intersecting microtubules was counted. The cuticular plate thickness was measured as the average vertical distance from the lumenal membrane of the second row OHC through the dense-actin meshwork at the lumenal OHC cytoplasm at three locations below the center of the three stereocilia rows. This measurement was repeated for three samples for each condition and compared using the sample mean and pooled standard deviation. To calculate the average inner hair cell-to-outer hair cell (ITO) distance as previously described (Jacques et al., 2007), the horizontal distance from the lateral side of the IHC to medial side of the first OHC was measured in 2 basal and 2 apical samples from 2 animals for each condition at 1 μm, 3 μm, and 5 μm distances from the lumenal surface of the PC. To quantify the morphology of OHCs, measurements of OHC length and width were also made. For all measurements, the mean, standard deviation, and standard error of the mean were calculated for each condition. Analysis of statistical significance was determined using student's T-test.

2.8 IMMUNOHISTOCHEMISTRY

2.8.1 Performed on Sectioned Tissues

Samples were fixed in 4% paraformaldehyde for 4 hours, rinsed, passed through an increasing sucrose gradient from 5-30%, embedded in OCT (Sakura, New York, USA) and cryosectioned at 12 μm thickness. Sections were permeabilized with 0.2% Tween-20 in 1X PBS, followed by blocking with 10% normal horse serum and incubated overnight in primary antibody (acetylated tubulin, Sigma, 1:750; $p75^{ntr}$,

Covance, 1:1000; ZO-1, Millipore, 1:1000; S100-A1, Neomarkers, Kalamazoo, Michigan, USA, 1:500; CD44, BD Pharmigen, Franklin Lakes, New Jersey, USA, 1:200; p-Cofilin, Santa Cruz Biotechnology, Santa Cruz, California, USA, 1:500) at 4°C. Primary antibodies were detected using either Alexa Fluor 488 or 546 (Invitrogen, 1:1000) conjugated secondary antibodies. Directly conjugated Phalloidin 633 (Invitrogen, 1:5000) was applied to all samples. To localize prosensory markers in embryonic stages of development, tissues were prepared as mentioned but fixed overnight at 4˚C and the following antibodies were applied: anti-Sox2 (Santa Cruz Biotechnologies, 1:250), anti-Myosin 6 (Proteus, 1:1000), anti-β-tubulin III (TuJ1) (Sigma-Aldrich, 1:250), anti-Jagged1 (Santa Cruz Biotechnologies, 1:250), anti-Prox1 (Covance, 1:400), anti-$p75^{ntr}$ (Millipore, 1:500), anti- $p27^{Kip1}$ (Neomarkers, 1:300), anti-Islet1 (Abcam, 1:250), anti-Atoh1 (Driver et al., In press). Primary antibody labeling was detected by incubation for one hour at room temperature using Alexa 546, 488, or 633-conjugated secondary antibodies (Invitrogen, 1:1000). Filamentous actin was detected using fluorophore-conjugated Phalloidin (Invitrogen, 1:200).

2.8.2 Performed on Whole-Mount Tissues

Cochleae prepared for whole mount immunohistochemistry differed in that samples were fixed for 2 hours at 4˚C and were labeled with a primary antibody (acetylated tubulin, Sigma, 1:750; $p75^{ntr}$, Covance, Princeton, New Jersey, USA, 1:750; ZO-1, Millipore, 1:1000; β-tubulin I&II, Sigma, 1:750; S100-A1, Neomarkers, Kalamazoo, Michigan, USA, 1:1000). Directly conjugated Phalloidin 633 (Invitrogen, 1:5000) was applied to all samples. Samples were mounted in Fluoromount-G (Southern Biotech) beneath No. 1½ glass coverslips (Corning, New York, USA) adhered with nail polish.

2.8.3 Image Acquisition, Processing, and Quantification

All fluorescence images were acquired at room temperature with LSM 510 acquisition software as 12 µm Z-stacks with 1 µm optical sectioning using a Zeiss 510 LSM Confocal Microscope with 40X oil objective (NA 1.3, WD= 0.21 mm, ∞ 0.17, Plan-Neofluar, Zeiss). Using line scan analysis, fluorescence intensity was measured from projected Z-stacks with ImageJ (Rasband, 1997) analysis software in 2 µm areas at the lumenal surfaces of both PCs and OHCs, as this region was previously observed with Transmission Electron Microscopy to maintain a homogeneous cell cytoplasm from E16 through P5. To measure relative fluorescence intensity in whole-mount samples, a 20 μm^3 average intensity z-projection was reconstructed using ImageJ analysis software (Rasband, 1997). Average gray values (mean±s.e.m. arbitrary units, AU) were calculated from 36 cells repeated for six animals. Average fluorescence intensity (mean±s.e.m. A.U.) was calculated from 6 samples, and compared using student's T-test. To quantify the difference in microtubules within OHCs, OHCs were first identified by row as containing stereocilia, and then were counted as positive or negative for β-Tubulin I&II fluorescence, as untreated OHCs contained β-Tubulin I&II at all time-points measured. Then the percent of positively labeled OHCs per culture (mean±s.e.m.) was calculated and compared between control and Fgf2- or SU5402-treated conditions. To quantify the overlap between prosensory markers, phalloidin labeling was used to identify the overall width of the cochlear duct. Cross-sections (base or apex) also labeled with prosensory markers were quantified as a percentage of width relative to overall width. Measurements were repeated on 7-10 sections of a given region (base or apex) to generate normalized expression profile histograms for each prosensory marker.

3 RESULTS

3.1 PAPER I

As mentioned in the Introduction, previous research has suggested a cellular basis for the observed radial gradient in basilar membrane stiffness (Emadi et al., 2004). The aim of **Paper I** was to determine if differences in cell mechanical properties arise during cochlear development. Therefore, we adapted cochlear explant cultures for atomic force microscopy to measure the Ym of OHCs and PCs during development. We found that at Embryonic day E16, OHCs and PCs have similar cell surface mechanical properties both at the basal and apical regions of the cochlea. However, by P0, we found distinct distributions of OHC and PC stiffness. Finally, by P5, we observed increasing stiffness in PCs from basal to apical regions of the cochlea. This suggested that cytoskeletal components, mainly actin filaments and microtubules, are developing within the cell cytoplasm and contributing to the mechanical properties of these cells. To test this hypothesis, we applied pharmacological treatment with either Latrunculin A or Jasplakinolide to disrupt the dynamics of the actin cytoskeleton. Treatment with Latrunculin A destabilized actin filaments and significantly decreased Ym of OHCs but not PCs. Treatment with Jasplakinolide stabilized actin filaments and significantly increased Ym of both OHCs and PCs. Interestingly, disruption of Myosin II function with Blebbistatin treatment at P0 significantly softened OHCs but significantly stiffened PCs. Taken together, these data suggest that actin directly impacts OHC surface mechanical properties and indirectly impacts PC stiffness.

As reported in **Paper I**, based on transmission electron microscopy studies, PCs at postnatal stages develop bundled arrays of microtubules that occupy the majority of the cytoplasm in adult tissues (Souter et al., 1998). To test the impact of microtubule development on cell surface mechanical properties, we treated cochlear explant cultures with either Nocodazole or Taxol. Treatment with Nocodazole depolymerized microtubules and significantly decreased Ym of OHCs but not PCs at P0. However, by P5, Nocodazole significantly decreased Ym of PCs but not OHCs. Treatment with Taxol disrupted microtubules and significantly decreased Ym of PCs but not OHCs at postnatal days 3 and 5. These data suggest that PC surface mechanical properties develop sensitivity to microtubules within the first postnatal week. It has been shown that other supporting cell types, such as Deiters' cells that interdigitate between OHCs, also contain microtubules (Slepecky, 1996). Therefore, we performed line-scan analysis of Ym to examine the cell mechanical properties throughout the second OHC row. We found heterogeneity in Ym along the longitudinal axis of the cochlea, and we proposed that this is due to the cellular heterogeneity of hair cells and supporting cells. Furthermore, this phenomenon is sensitive to microtubule disruption as treatment with Nocodazole was shown to decrease surface stiffness heterogeneity at P3.

Finally, we proposed that the Fibroblast growth factor (Fgf) signaling pathway modulates the time course of developing cell surface mechanical properties in the cochlea. Using fluorescence immunohistochemistry, we found that cochlear explant cultures treated with Fgf2, which stimulates all Fgf receptors, significantly decreased OHC and PC filamentous actin, while treatment with SU5402, which inhibits all Fgf receptors, significantly increased OHC filamentous actin. This disruption of actin in Fgf2 treated cultures may explain in part the observed softening of OHCs and PCs. To begin to understand the downstream mechanism underlying the functional changes with Fgf2 treatment, cochlear explant cultures were treated with Fgf2 and one of the

following: Rho-associated kinase inhibitor Y27632, mitogen-activated threonine\tyrosine kinase (MEK) inhibitor U0126, or c-Jun N-terminal kinase inhibitor SP60012. Only treatment combining Fgf2 with Y27632 significantly increased both OHC and PC surface stiffness at P3 when compared to cultures treated with Fgf2 alone. Treatments combining Fgf2 with either U0126 or SP60012 also increased PC stiffness when compared to cultures treated with Fgf2 alone, but this difference was not statistically significant.

3.2 PAPER II

To understand which Fgf-receptor(s) may contribute to the changes in cell surface mechanical properties observed in **Paper I**, we took advantage of an *in vivo* mouse model deficient in Fgf-receptor 3 (Fgfr3) (Colvin et al., 1996; Hayashi et al., 2007; Puligilla et al., 2007). The aim of **Paper II** was to determine if this receptor disrupts cell mechanics and if so then to outline the mechanism by which Fgf-receptor 3 might disrupt the cytoskeleton of the affected cell type(s). Previously, it was reported that *Fgfr3*$^{-/-}$ mice have a 60 dB sound pressure level hearing loss (Colvin et al., 1996) and lack otoacoustic emissions (Puligilla et al., 2007). Therefore, we first wanted to examine OHC electromotility, as changes in electromotility may confound interpretation of any changes to OHC surface mechanical properties. Isolated OHCs were tested for changes in voltage-independent (linear) and voltage-dependent (non-linear) capacitance, as well as electrical charge transfer, and the membrane potential at the observed peak in capacitance. All parameters tested did not present a statistically significant difference between OHCs from *Fgfr3*$^{+/-}$ and *Fgfr3*$^{-/-}$ mice. This suggested that Fgfr3 does not change the development of motor and sensory functions of OHCs.

One possible cause of the deafness observed in mice and humans with mutations in Fgfr3 (Puligilla et al., 2007; Doherty et al., 2007) is the disruptions to supporting cell stiffness. Therefore, we examined the cell surface mechanical properties of OHCs and PCs in cochlear explant cultures from *Fgfr3*$^{+/-}$ and *Fgfr3*$^{-/-}$ mice. We found that both OHC and PC stiffness is significantly reduced in *Fgfr3*$^{-/-}$ relative to *Fgfr3*$^{+/-}$ conditions. The decreased PC stiffness was not surprising given the observed malformations in organization of the sensory epithelium, decreased microtubule formation and decreased inner hair cell-to-outer hair cell (ITO) distance. However, the decreased OHC stiffness was not expected given that these cells seemed to have apparently normal morphology and function. It is possible that the OHC cytoskeleton, or the OHC tight junctions between Deiters' cells that anchor cytoskeletal components, may be disrupted due to the patterning defects previously described in this tissue (Hayashi et al., 2007; Puligilla et al., 2007).

The observed impact of microtubule disruption on cell surface mechanical properties in Fgfr3-deficient mice led to the hypothesis that Fgf-signaling might regulate microtubule formation during cochlear development. To begin to understand the regulation by Fgf-signaling at the transcriptional level, RNA was isolated from cochlear explant cultures that had been treated with either Fgf2 or SU5402. A gene expression profile of 84 cytoskeletal regulators was generated with quantitative real-time PCR for each condition and compared to vehicle control. Five genes were found to be significantly up-regulated in Fgf2- or SU5402-treated conditions, which included three microtubule regulators. *Mapre2* showed a three-fold increase in gene expression in SU5402-treated conditions, *Mark2* showed a four-fold increase in gene expression in SU5402-treated conditions, and *Clasp2* showed a three-fold increase in gene expression

in Fgf2-treated conditions. Together, these data suggest that Fgf-signaling indirectly impacts microtubule formation by altering transcription of microtubule regulators.

3.3 PAPER III

Previous work has shown that the thyroid hormone signaling pathway has several points of interaction with Fgf-signaling (for review see Williams et al., 2007) and previously it was reported that thyroid hormone receptors transcriptionally regulate Fgf-receptor 1(Fgfr1) in developing osteoblasts (O'Shea et al., 2007). The aim of **Paper III** was to examine if thyroid hormone levels regulate Fgf-signaling during cochlear development. Therefore, we developed a treatment protocol to render mice hypothyroid *in vivo* at embryonic and postnatal stages of development. We found increased mRNA expression of *Fgfr1* and *Fgfr3* in hypothyroid cochleae relative to control conditions. Using *in situ* hybridization, we localized the increase in *Fgfr1* to supporting cells of the greater epithelial ridge. We also observed a delayed down-regulation of *Fgfr3* in OHCs. This suggested that the phenotypic developmental delay seen in cases of hypothyroidism may contribute to cell shape and cell structural changes in the cochlea.

To characterize this developmental delay at the cellular level, we examined the protein localization of PC markers with immunohistochemistry in control and hypothyroid cochleae. We found that onset of calcium binding protein S100-A1 at E16, and down-regulation of neurotrophin receptor p75 ($p75^{ntr}$) at P3 were delayed in hypothyroid cochleae relative to control conditions. Furthermore, a decrease in CD44 expression, a marker of differentiated PCs, was observed in hypothyroid cochleae at P6. To examine the impact of delayed differentiation on the cytoskeleton, we used transmission electron microscopy to compare actin filament and microtubule formation in hypothyroid and control cochleae. We found fewer microtubules in hypothyroid cochleae, and found defects in OHC morphology. To quantify this difference in OHCs, we calculated the cell width-length ratio and compared between hypothyroid and control conditions. We found a significantly increased width-length ratio in hypothyroid OHCs when compared to control conditions. Using immunohistochemistry, we observed a reduction in acetylated tubulin in hypothyroid supporting cells. These experiments showed that thyroid hormone levels contributed to the developing cytoskeleton of OHCs and PCs, and therefore may also disrupt cell mechanical properties.

To test the functional consequences of hypothyroidism, cochlear explant cultures at embryonic and postnatal stages were established for atomic force microscopy. We found that PC stiffness was significantly decreased at P5, which was expected given the significant reduction in microtubules. However, hypothyroid PCs were significantly stiffer when compared to control conditions at E16 and P0. In addition, hypothyroid OHCs showed a trend from E16 to P0 towards increased cell stiffness that was statistically significant relative to control conditions at P3. Together, these data raised the possibility that actin may also contribute to developing cell mechanical properties. Therefore, we treated hypothyroid cochlear explant cultures with Latrunculin A and proposed that disruptions to actin formation would decrease Ym. Indeed, both hypothyroid OHCs and PCs were significantly softer after treatment with Latrunculin A, supporting the consensus that uncontrolled actin formation was responsible in part for the aberrant increase in developing cell mechanical properties in hypothyroid conditions.

Finally, we explored the mechanism by which thyroid hormone induced actin-based stiffening in OHCs and PCs. As a first step, we profiled a panel of 84 cytoskeleton regulators for gene expression changes in hypothyroid conditions using quantitative real-time PCR. Since there were no statistically significant differences in cytoskeletal regulators between hypothyroid and control conditions, we examined potential signaling cascades downstream of the Fgf-signaling pathway. First, we identified increased phosphorylation of Fgf-receptors at E16 that persisted at P0. As mentioned in the **Introduction**, Fgf-receptors are members of a family of tyrosine kinase receptors that have been shown to act through four key signaling cascades, which include mitogen-activated kinase (MAPK), phosphoinositide 3-kinase (PI3K), signal transducer and activator of transcription (STAT), and phospholipase C-gamma (PLC-γ). We found that Lim-kinase (LIMK), an intermediary in the MAPK signaling cascade (Edwards et al., 1999) showed increased phosphorylation in hypothyroid relative to control conditions. LIMK has been shown to interact with key regulators of actin dynamics, including, but not limited to, cofilin. Phosphorylation of actin-depolymerizing factor cofilin was also significantly decreased in hypothyroid relative to control conditions. Decreased phosphorylation of cofilin has been shown to lead to an increase in actin filament formation (Marsick et al., 2010) by creating free barbed ends for polymerization, which may explain in part the stiffening of hypothyroid OHCs and PCs. In order to localize this difference in cofilin phosphorylation, we applied immunohistochemistry to cross-sectioned cochleae from hypothyroid and control conditions, using a commercially available antibody raised against phosphorylated cofilin. We found decreased phosphorylated cofilin in the nucleus of hypothyroid OHCs relative to controls. Taken together, these data suggest that altered cofilin activity may play a role in the increased actin-based stiffness in hypothyroid conditions.

3.4 PAPER IV

Specification of a population of prosensory cells with the ability to develop as hair cells or supporting cells is a key step in the development of the sensory epithelium. But the factors that specify this population of cells are only beginning to be understood. Here, we examined the expression of putative prosensory markers in the developing mouse cochlea. By E14.5 three prosensory markers were visible at mid-basal sections, Sox2, Jagged1, and Islet1. However, these markers had very little overlap when confocal images were examined in pseudo-overlay. The Sox2 immunopositive region was the most narrow and medially localized. The Jagged1 immunopositive region extends most laterally. By E13.5, Jagged1 expression had narrowed somewhat. At time points examined between E12.5 and E14.5, Islet1 expression was the broadest, overlapping with the Sox2-positive region and extending through the lateral epithelial ridge. Even at E14.5, Islet1 expression extends more laterally than either Sox2 or Jagged1. Interestingly, along this same time course, spiral ganglion fibers also developed along the cochlear duct, as detected by neuronal-specific β-tubulin III, before hair cell formation began. These results demonstrate that while Sox2 and Jagged1 are required for prosensory formation, they are not definitive markers of this domain, suggesting that other factors probably act to refine the prosensory domain beyond the expression of Sox2, Jagged1, and Islet1.

Beginning between E13.5 and E14.5, a subset of cells within the Sox2, Jagged1, and Islet1 domain become positive for the cell-cycle inhibitor, $p27^{Kip1}$. While not required for prosensory formation (Chen and Segil, 1999), expression of $p27^{Kip1}$ appears to be the most definitive marker for the prosensory domain. Expression of $p27^{Kip1}$ identifies the prosensory cells that have become post-mitotic from the non-

sensory regions of Kölliker's organ and the lateral epithelial ridge. By E14.5, supporting cell markers Prox1, a prospero-related homeodomain transcription factor, and neurotrophin receptor p75 ($p75^{ntr}$) were apparent at mid-basal regions of the cochlear duct and overlapped with the early prosensory markers Sox2, Jagged1, and Islet1. Both $p75^{ntr}$ and Prox1 are expressed in just the lateral two-thirds of the prosensory domain with a sharp medial border. Preliminary profiling of expression for Prox1 of $p75^{ntr}$ with the hair cell marker Atoh1 indicates that a majority of hair cells may arise from the approximately one-third of the prosensory domain that is negative for $p75^{ntr}$ and Prox1, but further analysis is required to confirm this possibility. By E15, overlap between Jagged1 and Sox2 had increased. Of particular interest, the overlap between Jagged1 and β-tubulin III may indicate the presumptive prosensory region along the cochlear duct.

Between E16 and P0, strong distinctions in marker expression become evident in sensory hair cells and non-sensory supporting cells. Beginning at E16, immunohistochemistry of cochlear cross-sections showed that $p75^{ntr}$ expression is down-regulated in most cells within the prosensory domain with the exception of developing pillar cells. Pillar cells, as well as most other supporting cells, also expressed both Sox2 and Jagged1. However, Jagged1 expression was down-regulated in the most lateral region of the organ of Corti. As expected, there was no overlap between Numb, an antagonist of Notch signaling, and Jagged1. It was interesting to note that while all Jagged1-positive cells were also Sox2-positive, not all Sox2-positive cells contained Jagged1. In contrast to the supporting cells, OHC expression of both Sox2 and Jagged1 was completely lost in Myosin 6-positive hair cells. Finally, Islet1 expression, maintained throughout embryonic development including P0, was similar to $p75^{ntr}$. There was an overlap observed between Islet1 and both Jagged1 and Sox2 expression profiles.

4 DISCUSSION AND FUTURE DIRECTIONS

4.1 PAPER I

With the adaptation of cochlear explant cultures to atomic force microscopy, we can quantify the material properties that resist deformation at the cellular level. This resolution was shown by our measurements of stiffness heterogeneity along OHC rows, which indicated that areas at cell-cell junctions have a higher Young's modulus (Ym) than the center of the cell. Furthermore, supporting Deiters' cells, which interdigitate between OHCs and are composed of primarily microtubules, showed a higher resistance to deformation when compared to OHCs in the same row at postnatal stages. This is a strong advantage of our technique as future experiments could assess the impact of developing tight and adherens junctions on hair cell and supporting cell stiffness. Furthermore, cell junctions often provide stability points to connect actin and microtubule networks, and could be explored in more detail to understand the relationship between these cytoskeletal components in dictating the heterogeneity of cell surface mechanical properties.

This high resolution of our technique has also limited the extent to which AFM can probe the dense cytoskeletal network deep within the OHC cytoplasm. The indentation depth for this technique measured 1.5 μm, which may limit the extent to which our measurements of Ym represented the stiffness of the entire OHC. This depth was critical to minimize the impact of cell membrane mechanics on measurements of cell stiffness (Sen et al., 2005) and it was clear from transmission electron micrographs that this indentation depth remained homogeneous throughout the developmental time course under consideration. It would be interesting to compare these measurements of individual cell stiffness to the mechanics of the reticular lamina that forms after P10 (Leonova and Raphael, 1997) and forms a critical barrier between endolymph and perilymph fluids (Bohne and Rabbitt, 1983). This assessment of cell surface mechanical properties ought to be considered in context as a critical first step, and could well be applied to modeling and mechanics studies of the main events in morphogenesis, namely the cellular exertion of force during cellular protrusion and cell motility, and the cellular resistance to deformation during development.

4.2 PAPER II

This study reaffirms the utility of the *Fgfr3*$^{-/-}$ mouse as a model to study the impact of supporting cells on the mechanics of hearing. As OHC function appeared normal, new considerations should be raised to better understand the 60 dB sound pressure level hearing loss and lack of otoacoustic emissions. One possibility may be that a loss of endocochlear potential in these mice may be contributing to OHC function *in vivo*. However, a loss of endocochlear potential in these animals seems unlikely, given that previous cases of disruption to potassium recycling result in a degradation of OHCs (Okano and Iwai, 1975; Bohne and Rabbitt, 1983), which was not seen in *Fgfr3*$^{-/-}$ mice (Colvin et al., 1996; Hayashi et al., 2007; Puligilla et al., 2007). Another more likely contribution comes from the underdeveloped supporting cells, which fail to form the fluid filled Spaces of Nuel (Souter et al., 1997) and inner and outer Tunnels of Corti (Scott, 1909; Lim and Anniko, 1985). The field of fluid flow in the cochlear duct is still largely unexplored, but stroboscopic image analyses have implicated fluid flow through the tunnel of Corti as contributing to hearing function (Karavitaki and Mountain, 2007). Furthermore, the fluid spaces of Nuel are thought to be a permissive requirement for

OHC amplification *in vivo* (Zagadou and Mountain, 2012). Together, this work supports the need for a better understanding of the process by which non-sensory supporting cells amplify or dampen sensory hair cell mechanotransduction. In this study, we identified five candidate genes (*Clasp2, Crk, Cyfip1, Mapre2, Mark2*) that may be responsible for supporting cell development and in particular for the morphological changes of supporting cells during postnatal stages of maturation. Interestingly, the majority of genes with significantly increased fold-change expression were directly or indirectly linked to microtubule formation (Mimori-Kiyosue et al., 2005; Sapir et al., 2008; Vitre et al., 2008). Future experiments localizing these candidates to the sensory epithelium with *in situ* hybridization or immunohistochemistry, and interrogating these gene promoter and enhancer regions for putative regulatory sequences, would further establish the role for Fgf-signaling on microtubule formation.

In this thesis, measurements of the material properties of supporting cells were limited to supporting PCs and the surface of Deiters' cell processes in OHC row 2. However, the cochlear sensory epithelium after the onset of hearing contains 7 morphologically distinct subtypes of supporting cells, including border cells, phalangeal cells, inner and outer PCs, Deiters' cells, Hensen's cells and Claudius cells (Lim and Anniko, 1985; Slepecky et al., 1996). Current distinctions between these subtypes include the location of the supporting cell nucleus relative to the basilar membrane, and the positional identity of each cell within the sensory epithelium. Additional research characterizing supporting cell subtypes of developing epithelia would complement established morphological distinctions, and permit additional measurements of these cell surface mechanical properties *in vitro*. In **Paper II**, close examination of transmission electron micrographs in $Fgfr3^{+/-}$ and $Fgfr3^{-/-}$ cochleae led to the conclusion that both inner and outer PCs, as well as an inner phalangeal cell, were present in both genotypes. This was based primarily on the location of the cell type within the epithelium, as well as the position of the nucleus relative to the basilar membrane. Other interpretations could be that overproliferating phalangeal cells, or movements of non-sensory cells from Kölliker's organ, are recruited to maintain the interdigitation of hair cells and supporting cells characteristic of the auditory organ. Before a thorough characterization of this mouse model can be completed, new and unique supporting cell markers are necessary to identify sub-populations of supporting cells. One clue may be in candidates with some impact on nuclear positioning (Miller et al., 1998) or cell adhesion properties that mediate intercellular recognition signaling cascades (Simonneau et al., 2003).

4.3 PAPER III

As mentioned briefly in the **Introduction**, there are many distinct points of cross-talk between thyroid hormone signaling and fibroblast growth factor signaling pathways. The most direct regulation of thyroid hormone receptors occurs when these receptors bind transcriptional regulatory sequences in either promoter or enhancer regions that control target gene transcription (Weitzel, 2008). Previously, it was shown that treatment with thyroid hormones induced *Fgfr3* and *Fgfr1* expression in osteoblast cells lines (Barnard et al., 2005); the development of new techniques that include single-cell reporter assays in cochlear explant cultures might someday lend insight into a direct mechanism. In addition, thyroid hormones also have been shown to bind integrin receptors α_V and β_3 (Bergh et al., 2005), which induce downstream activation of MAPK signaling cascades. This receptor-independent regulation is an appealing mode of spatially controlled cross-talk given that the cochlea undergoes dynamic

expression of several integrin receptors that are responsible, in part, for Fgf-mediated cell growth (Toyama et al., 2005). Thyroid hormone receptors can also remain in the cell cytoplasm independent of ligand and have been shown to bind the regulatory subunit of PI3K (Kenessey and Ojamaa, 2006), which contains an SH2 domain capable of binding phosphorylated tyrosine residues (Songyang et al., 1993) such as those found on Fgf-receptors. Finally, thyroid hormones may have indirect control over Fgf-receptor activation by regulating the localization or bioavailability of heparin sulfate proteoglycans, as has been observed in developing bone tissue (Bassett et al., 2006). Overall, these several avenues of exploration would lead to further understanding of the cross-talk between these signaling pathways, and may provide additional biomarkers of thyroid hormone status in developing or developed tissues.

One major goal for the developmental biologist in the field of hearing research is to translate the understanding of cochlear development for the regeneration or repair of damaged sensory epithelia. As the adult mammalian cochlea does not regenerate (Collado et al., 2011), much attention has been placed on mechanisms with the potential to repair or delay death of hair cells and supporting cells (Taleb et al., 2008; Hinz et al., 2011). Precise control over the timing of cellular differentiation, including the ability to de-differentiate adult tissues, could open new avenues for therapeutic intervention. In many ways, the developmental delay seen in hypothyroid conditions *in vivo* is similar to the under-differentiation of developing cochlear explant cultures treated with Fgf2 *in vitro*. While still unexplored, it may be possible to force the differentiation of Fgf2 treated explants or $Fgfr3^{-/-}$ mice through the delivery of thyroid hormones. It would be very interesting to understand the extent to which these same mechanisms are active in adult or aging systems. Fgf2 treated explants *in vitro* lose the potential to de-differentiate by P5, yet it is still uncertain if Fgf signaling persists as there is evidence for a persistent expression of Fgf-receptors in the cochlea (Pirvola et al., 1995). Even if these mechanisms are not readily accessible in the aging cochlea, future progress into genetic and epigenetic methods may shed new light on how best to harness the key growth factors from development to extend the hearing function of the aging cochlea.

4.4 PAPER IV

The identification of a homogenous measurement of Ym in the cochlear sensory epithelium at E16 in **Paper I** suggests that the prosensory region has not yet differentiated to distinguish hair cell from support cell stiffness. In **Paper IV** we have been able to refine the definition of the presumptive organ of Corti using multiple markers of the prosensory domain, such as Jagged1 and Sox2. This systematic investigation raises new possibilities for investigators interested in applying the cochlear epithelium to modernized single-cell analyses, which would require a high-throughput enrichment of clonal cell populations. Furthermore, it would be interesting to examine the stiffness differences between the prosensory region of the cochlear duct and other non-sensory regions as early as E13. Recent work identifying new cell-surface receptors in the prosensory domain suggests that the cell membranes of prosensory and nonsensory cells may have different material properties. To examine the cell membrane with an AFM, additional experiments to optimize the efficiency of force-imaging are essential. Currently, topography of epithelial cells can be examined with a commercial AFM in tapping mode, but image acquisition takes minutes. This long time scale leads to either a sacrifice of high spatial resolution of AFM, or a degradation of the tissue if multiple images are acquired on the same tissue. Advancements in ion-conductance scanning AFM (Novak et al., 2009) have taken the

first step to minimizing the disadvantage of low spatial resolution, and may be able to quantify the density of cell surface receptors that show differential expression in prosensory and nonsensory regions of the cochlear duct.

There is growing evidence that mechanical cues may direct differentiation in resident stem cell populations of several human and mouse tissues (Engler et al., 2006). But the impact of substrate stiffness on prosensory cell specification has not yet been tested. The expression of $p75^{ntr}$ in a subset of supporting cells, namely the PCs, is a marker of a less-differentiated state in the cochlea (Jacques et al., 2007) and suggests that these cells may have a yet underappreciated plasticity that remains after cell fate specification. Indeed, expression of $p75^{ntr}$ in Schwann cells (Soilu-Hänninen et al., 1999) has been observed in cases of neuron damage and proliferation (King et al., 2000). While it may be possible to extend expression of this neurotrophin receptor by altering the time course of exposure to growth factors or thyroid hormones, it remains to be seen how expression of $p75^{ntr}$ alters the expression of cell cycle controls or correlates with proliferation in the cochlea. Additional experiments aimed at altering the mechanical properties of the basilar membrane substrate beneath this sensory epithelium may work in concert with differentiation factors such as $p75^{ntr}$ to control the proliferation of single-cell populations. Alternatively, with the introduction of hair cell-like stem cells (Oshima et al., 2010) and cochlear progenitor cell lines (Kwan et al., in preparation) the substrate matrix elasticity could be experimentally altered to determine which substrate stiffness promotes, permits, or inhibits expression of $p75^{ntr}$. Both lines of research could lend insight into the pathways of differentiation that could be applied towards regrowth or repair of the cochlear sensory epithelium.

5 ACKNOWLEDGEMENTS

First, I would like to thank my KI and NIH mentors for collaborating on this PhD project. Mats, thank you for your collaboration and for introducing me to Anders. You were my ambassador to science in Sweden, and you set into motion my transformation. I am so grateful for this opportunity. Anders, thank you for sharing with me your ideas, your ambitions, and your experiences. You introduced me to the temporal bone preparation, and you challenged me to refine my critical thinking in ways that improved my science. Thank you also to your lab, Anna's and Petri's, for being my Swedish family. You shared with me another way to look at life in the lab, and added a more international perspective to the process of research. Richard, thank you for being there in crucial moments that made me feel like my work was important. Thank you for making yourself available for Christmas emails, evening meetings, and afternoon discussions. Matt, thank you for trusting me to go in my own direction. Mentors wear many hats and you often needed to wear those hats all at once. I am so glad you could think clearly and teach me to prioritize. You cared for my success in science and my well-being even when I forgot to do so.

Ron, you had never-ending patience with me. Thank you and Ya-Xian for sharing your EM experience with me; this look into the cell gave me a whole new outlook on science. Thank you for discussions and teaching—your passion for science is contagious and I will never tire of exploring the cell.

To my benchmates: Núria, thank you for teaching me how to be a graduate student. You made me stronger with positive feedback and answered the questions I was still too young to think about. Zoe, thank you for exemplifying the strength I need to find in myself to keep calm and carry on. And that when times get tough, put the kettle on! Stefan, for doing everything to make my time in Sweden productive, questioning my thinking and laying out my options. You thickened my skin for science, and your investment is something I strive to pay forward every day.

To the people that brought me out of my shell in the lab: Betsy, thank you for instilling birthday wishes and asking me questions in my lab meetings. I would go home knowing I did well because you asked me something. Tom, organizing baseball outings got me some sun and some helpful discussions. Weise, thank you for encouraging me to have different perspectives about my materials and methods. Jessica and Sonya, thank you for your patience as I tried to absorb all I could about cochlear mechanics. For all the labmates who left before me, Alain, Kala, Bonnie, Norio, Taka, Helen, Laura, Lydia, Jamie, and Luca, you made life in lab more fun! For the newest additions to lab, I am sad to be leaving so soon after meeting you.

Mom and dad! Your eyes say that you can see that I love this. Thank you for investing yourselves to make me happy. Andrew, my husband, you are my balance and you continue to let me give of myself. You are the strength behind my endeavors.

This work was supported by the NIDCD Intramural Research Program. Thanks also to the Office of the Director at NIH, and Sharon Milgram at OITE, for the Intramural Fellowship to Promote Diversity. Thanks to Dr. Robert Harris and the administration of the NIH-Karolinska Graduate Program. My teaching efforts were supported by Dr. Maurice Godfrey, Dr. Carla Easter, the Rosebud Indian Reservation of South Dakota, USA, and the FAES.

6 REFERENCES

Alford BR, Ruben RJ. Physiological, behavioral and anatomical correlates of the development of hearing in the mouse. Ann Otol Rhinol Laryngol. 1963 Mar;72:237-47.

Avraham KB, Hasson T, Steel KP, Kingsley DM, Russell LB, Mooseker MS, Copeland NG, Jenkins NA. The mouse Snell's waltzer deafness gene encodes an unconventional myosin required for structural integrity of inner ear hair cells. Nat Genet. 1995 Dec;11(4):369-75.

Barnard JC, Williams AJ, Rabier B, Chassande O, Samarut J, Cheng SY, Bassett JH, Williams GR. Thyroid hormones regulate fibroblast growth factor receptor signaling during chondrogenesis. Endocrinology. 2005 Dec;146(12):5568-80.

Bassett JH, Swinhoe R, Chassande O, Samarut J, Williams GR. Thyroid hormone regulates heparan sulfate proteoglycan expression in the growth plate. Endocrinology. 2006 Jan;147(1):295-305.

Bell TJ, Oberholtzer JC. cAMP-induced auditory supporting cell proliferation is mediated by ERK MAPK signaling pathway. J Assoc Res Otolaryngol. 2010 Jun;11(2):173-85.

Belyantseva IA, Boger ET, Naz S, Frolenkov GI, Sellers JR, Ahmed ZM, Griffith AJ, Friedman TB. Myosin-XVa is required for tip localization of whirlin and differential elongation of hair-cell stereocilia. Nat Cell Biol. 2005 Feb;7(2):148-56.

Ben-Arie N, McCall AE, Berkman S, Eichele G, Bellen HJ, Zoghbi HY. Evolutionary conservation of sequence and expression of the bHLH protein Atonal suggests a conserved role in neurogenesis. Hum Mol Genet. 1996 Sep;5(9):1207-16.

Bergh JJ, Lin HY, Lansing L, Mohamed SN, Davis FB, Mousa S, Davis PJ. Integrin alphaVbeta3 contains a cell surface receptor site for thyroid hormone that is linked to activation of mitogen-activated protein kinase and induction of angiogenesis. Endocrinology. 2005 Jul;146(7):2864-71.

Bermingham NA, Hassan BA, Price SD, Vollrath MA, Ben-Arie N, Eatock RA, Bellen HJ, Lysakowski A, Zoghbi HY. Math1: an essential gene for the generation of inner ear hair cells. Science. 1999 Jun 11;284(5421):1837-41.

Bermingham-McDonogh O, Oesterle EC, Stone JS, Hume CR, Huynh HM, Hayashi T. Expression of Prox1 during mouse cochlear development. J Comp Neurol. 2006 May 10;496(2):172-86.

Bernstein BW, Bamburg JR. ADF/cofilin: a functional node in cell biology. Trends Cell Biol. 2010 Apr;20(4):187-95.

Bilodeau GG. Regular pyramid punch problem. J Appl Mech. 1992 59:519-23.

Bohne BA, Rabbitt KD. Holes in the reticular lamina after noise exposure: implication for continuing damage in the organ of Corti. Hear Res. 1983 Jul;11(1):41-53.

Bradley DJ, Towle HC, Young WS 3rd. Alpha and beta thyroid hormone receptor (TR) gene expression during auditory neurogenesis: evidence for TR isoform-specific transcriptional regulation in vivo. Proc Natl Acad Sci U S A. 1994 Jan 18;91(2):439-43.

Briscoe BJ, Sebastian KS, Adams MJ. The effect of indenter geometry on the elastic response to indentation. J Phys. D: Appl. Phys. 1994 27:1156-62.

Brors D, Hansen S, Mlynski R, Volkenstein S, Aletsee C, Sendtner M, Ryan AF, Dazert S. Spiral ganglion outgrowth and hearing development in p75-deficient mice. Audiol Neurootol. 2008;13(6):388-95. Epub 2008 Jul 29.

Brown-Grant K. Further studies of the metabolism of thyroxine and 3,5,3' - triiodothyronine in the guinea-pig. J Physiol. 1967 Jul;191(1):167-76.

Burns R, O'Herlihy C, Smyth PP. The placenta as a compensatory iodine storage organ. Thyroid. 2011 May;21(5):541-6.

Coling DE, Espreafico EM, Kachar B. Cellular distribution of myosin-V in the guinea pig cochlea. J Neurocytol. 1997 Feb;26(2):113-20.

Collado MS, Thiede BR, Baker W, Askew C, Igbani LM, Corwin JT. The postnatal accumulation of junctional E-cadherin is inversely correlated with the capacity for supporting cells to convert directly into sensory hair cells in mammalian balance organs. J Neurosci. 2011 Aug 17;31(33):11855-66.

Colvin JS, Bohne BA, Harding GW, McEwen DG, Ornitz DM. Skeletal overgrowth and deafness in mice lacking fibroblast growth factor receptor 3. Nat Genet. 1996 Apr;12(4):390-7.

Chang KH, Chen Y, Chen TT, Chou WH, Chen PL, Ma YY, Yang-Feng TL, Leng X, Tsai MJ, O'Malley BW, Lee WH. A thyroid hormone receptor coactivator negatively regulated by the retinoblastoma protein. Proc Natl Acad Sci U S A. 1997 Aug 19;94(17):9040-5.

Chen JD, Evans RM. A transcriptional co-repressor that interacts with nuclear hormone receptors. Nature. 1995 Oct 5;377(6548):454-7.

Chen P, Segil N. p27kip1 links cell proliferation to morphogenesis in the developing organ of corti. Development. 1999 Apr;126(8):1581-90.

Conti MA, Even-Ram S, Liu C, Yamada KM, Adelstein RS. Defects in cell adhesion and the visceral endoderm following ablation of nonmuscle myosin heavy chain II-A in mice. J Biol Chem. 2004 Oct 1;279(40):41263-6.

Dabdoub A, Puligilla C, Jones JM, Fritzsch B, Cheah KS, Pevny LH, Kelley MW. Sox2 signaling in prosensory domain specification and subsequent hair cell differentiation in the developing cochlea. Proc Natl Acad Sci U S A. 2008 Nov 25;105(47):18396-401.

Dallos P. Overview: cochlear neurobiology. Eds Dallos P, Popper AN, Fay RR. The Cochlea. Springer Handbook of Auditory Research. 1996 8:1-43.

de Jesus LA, Carvalho SD, Ribeiro MO, Schneider M, Kim SW, Harney JW, Larsen PR, Bianco AC. The type 2 iodothyronine deiodinase is essential for adaptive thermogenesis in brown adipose tissue. J Clin Invest. 2001 Nov;108(9):1379-85.

Desai U, Rosen H, Mulliken JB, Gopen Q, Meara JG, Rogers GF. Audiologic findings in Pfeiffer syndrome. J Craniofac Surg. 2010 Sep;21(5):1411-8.

Desvergne B. How do thyroid hormone receptors bind to structurally diverse response elements? Mol Cell Endocrinol. 1994 Apr;100(1-2):125-31.

Dimitriadis EK, Horkay F, Maresca J, Kachar B, Chadwick RS. Determination of elastic moduli of thin layers of soft material using the atomic force microscope. Biophys J. 2002 May;82(5):2798-810.

Doherty ES, Lacbawan F, Hadley DW, Brewer C, Zalewski C, Kim HJ, Solomon B, Rosenbaum K, Domingo DL, Hart TC, et al. Muenke syndrome (FGFR3-related craniosynostosis): expansion of the phenotype and review of the literature. Am J Med Genet A. 2007 Dec 15;143A(24):3204-15.

Driver EC, Sillers L, Rose M, Zoghbi HY, Kelley MW. The Atoh1-Expressing Cell Lineage Develops Into Both Hair Cells and Supporting Cells. Dev Biol. 2012. (in press)

Emadi G, Richter CP, Dallos P. Stiffness of the gerbil basilar membrane: radial and longitudinal variations. J Neurophysiol. 2004 Jan;91(1):474-88.

Engler AJ, Sen S, Sweeney HL, Discher DE. Matrix elasticity directs stem cell lineage specification. Cell. 2006 Aug 25;126(4):677-89.

Esfandiari A, Courtin F, Lennon AM, Gavaret JM, Pierre M. Induction of type III deiodinase activity in astroglial cells by thyroid hormones. Endocrinology. 1992 Oct;131(4):1682-8.

Etournay R, Lepelletier L, Boutet de Monvel J, Michel V, Cayet N, Leibovici M, Weil D, Foucher I, Hardelin JP, Petit C. Cochlear outer hair cells undergo an apical circumference remodeling constrained by the hair bundle shape. Development. 2010 Apr;137(8):1373-83.

Forge A. Structural features of the lateral walls in mammalian cochlear outer hair cells. Cell Tissue Res. 1991 Sep;265(3):473-83.

Forman BM, Casanova J, Raaka BM, Ghysdael J, Samuels HH. Half-site spacing and orientation determines whether thyroid hormone and retinoic acid receptors and related factors bind to DNA response elements as monomers, homodimers, or heterodimers. Mol Endocrinol. 1992 Mar;6(3):429-42.

Forrest D, Erway LC, Ng L, Altschuler R, Curran T. Thyroid hormone receptor beta is essential for development of auditory function. Nat Genet. 1996 Jul;13(3):354-7.

Fridberger A, Von Tiedemann M, Flock A, Flock B, Ofverstedt LG, Skoglund U. Three-dimensional structure of outer hair cell pillars. Acta Otolaryngol. 2009 Sep;129(9):940-5.

Frolenkov GI, Mammano F, Belyantseva IA, Coling D, Kachar B. Two distinct Ca(2+)-dependent signaling pathways regulate the motor output of cochlear outer hair cells. J Neurosci. 2000 Aug 15;20(16):5940-8.

Furness DN, Katori Y, Mahendrasingam S, Hackney CM. Differential distribution of beta- and gamma-actin in guinea-pig cochlear sensory and supporting cells. Hear Res. 2005 Sep;207(1-2):22-34.

Galton VA. The roles of the iodothyronine deiodinases in mammalian development. Thyroid. 2005 Aug;15(8):823-34.

Gestwa G, Wiechers B, Zimmermann U, Praetorius M, Rohbock K, Köpschall I, Zenner HP, Knipper M. Differential expression of trkB.T1 and trkB.T2, truncated trkC, and p75(NGFR) in the cochlea prior to hearing function. J Comp Neurol. 1999 Nov 8;414(1):33-49.

Gierer A, Meinhardt H. Donald S. Cohen. ed. "Biological Pattern Formation Involving Lateral Inhibition". Some Mathematical Questions in Biology VI: Mathematical Aspects of Chemical and Biochemical Problems and Quantum Chemistry (American Mathematical Society) 7. 1974.

Glass CK, Franco R, Weinberger C, Albert VR, Evans RM, Rosenfeld MG. A c-erb-A binding site in rat growth hormone gene mediates trans-activation by thyroid hormone. Nature. 1987 Oct 22-28;329(6141):738-41.

Gros J, Hu JK, Vinegoni C, Feruglio PF, Weissleder R, Tabin CJ. WNT5A/JNK and FGF/MAPK pathways regulate the cellular events shaping the vertebrate limb bud. Curr Biol. 2010 Nov 23;20(22):1993-2002.

Hallenbeck PL, Marks MS, Lippoldt RE, Ozato K, Nikodem VM. Heterodimerization of thyroid hormone (TH) receptor with H-2RIIBP (RXR beta) enhances DNA binding and TH-dependent transcriptional activation. Proc Natl Acad Sci U S A. 1992 Jun 15;89(12):5572-6.

Hallworth R, McCoy M, Polan-Curtain J. Tubulin expression in the developing and adult gerbil organ of Corti. Hear Res. 2000 Jan;139(1-2):31-41.

Hayashi T, Cunningham D, Bermingham-McDonogh O. Loss of Fgfr3 leads to excess hair cell development in the mouse organ of Corti. Dev Dyn. 2007 Feb;236(2):525-33.

Hayashi T, Ray CA, Younkins C, Bermingham-McDonogh O. Expression patterns of FGF receptors in the developing mammalian cochlea. Dev Dyn. 2010 Mar;239(3):1019-26.

Heery DM, Kalkhoven E, Hoare S, Parker MG. A signature motif in transcriptional co-activators mediates binding to nuclear receptors. Nature. 1997 Jun 12;387(6634):733-6.

Hinz A, Lee S, Jacoby K, Manoil C. Membrane proteases and aminoglycoside antibiotic resistance. J Bacteriol. 2011 Sep;193(18):4790-7.

Hoch RV, Soriano P. Context-specific requirements for Fgfr1 signaling through Frs2 and Frs3 during mouse development. Development. 2006 Feb;133(4):663-73.

Holley MC, Ashmore JF. Spectrin, actin and the structure of the cortical lattice in mammalian cochlear outer hair cells. J Cell Sci. 1990 Jun;96 (Pt 2):283-91.

Holley MC, Kalinec F, Kachar B. Structure of the cortical cytoskeleton in mammalian outer hair cells. J Cell Sci. 1992 Jul;102 (Pt 3):569-80.

Hörlein AJ, Näär AM, Heinzel T, Torchia J, Gloss B, Kurokawa R, Ryan A, Kamei Y, Söderström M, Glass CK, et al. Ligand-independent repression by the thyroid hormone receptor mediated by a nuclear receptor co-repressor. Nature. 1995 Oct 5;377(6548):397-404.

Horn S, Heuer H. Thyroid hormone action during brain development: More questions than answers. Mol Cell Endocrinol. 2010 Feb 5;315(1-2):19-26.

Humphrey D, Duggan C, Saha D, Smith D, Käs J. Active fluidization of polymer networks through molecular motors. Nature. 2002 Mar 28;416(6879):413-6.

Ibrahimi OA, Zhang F, Hrstka SC, Mohammadi M, Linhardt RJ. Kinetic model for FGF, FGFR, and proteoglycan signal transduction complex assembly. Biochemistry. 2004 Apr 27;43(16):4724-30.

Itoh N, Ornitz DM. Fibroblast growth factors: from molecular evolution to roles in development, metabolism and disease. J Biochem. 2011 Feb;149(2):121-30.

Jacques BE, Montcouquiol ME, Layman EM, Lewandoski M, Kelley MW. Fgf8 induces pillar cell fate and regulates cellular patterning in the mammalian cochlea. Development. 2007 Aug;134(16):3021-9.

Jamesdaniel S, Hu B, Kermany MH, Jiang H, Ding D, Coling D, Salvi R. Noise induced changes in the expression of p38/MAPK signaling proteins in the sensory epithelium of the inner ear. J Proteomics. 2011 Dec 21;75(2):410-24.

Jensen-Smith HC, Eley J, Steyger PS, Ludueña RF, Hallworth R. Cell type-specific reduction of beta tubulin isotypes synthesized in the developing gerbil organ of Corti. J Neurocytol. 2003 Feb;32(2):185-97.

Kaplan MM, Yaskoski KA. Effects of congenital hypothyroidism and partial and complete food deprivation on phenolic and tyrosyl ring iodothyronine deiodination in the rat brain. Endocrinology. 1982 Mar;110(3):761-7.

Karavitaki KD, Mountain DC. Evidence for outer hair cell driven oscillatory fluid flow in the tunnel of corti. Biophys J. 2007 May 1;92(9):3284-93.

Katz RW, Koenig RJ. Specificity and mechanism of thyroid hormone induction from an octamer response element. J Biol Chem. 1994 Jul 22;269(29):18915-20.

Kelley MW, Driver EC, Puligilla C. Regulation of cell fate and patterning in the developing mammalian cochlea. Curr Opin Otolaryngol Head Neck Surg. 2009 Oct;17(5):381-7.

Kenessey A, Ojamaa K. Thyroid hormone stimulates protein synthesis in the cardiomyocyte by activating the Akt-mTOR and p70S6K pathways. J Biol Chem. 2006 Jul 28;281(30):20666-72.

Kiernan AE, Pelling AL, Leung KK, Tang AS, Bell DM, Tease C, Lovell-Badge R, Steel KP, Cheah KS. Sox2 is required for sensory organ development in the mammalian inner ear. Nature. 2005 Apr 21;434(7036):1031-5.

Kiernan AE, Xu J, Gridley T. The Notch ligand JAG1 is required for sensory progenitor development in the mammalian inner ear. PLoS Genet. 2006 Jan;2(1):e4.

Kikuchi T, Kimura RS, Paul DL, Takasaka T, Adams JC. Gap junction systems in the mammalian cochlea. Brain Res Brain Res Rev. 2000 Apr;32(1):163-6.

Kimura RS. The ultrastructure of the organ of Corti. Int Rev Cytol. 1975;42:173-222.

King VR, Bradbury EJ, McMahon SB, Priestley JV. Changes in truncated trkB and p75 receptor expression in the rat spinal cord following spinal cord hemisection and spinal cord hemisection plus neurotrophin treatment. Exp Neurol. 2000 Oct;165(2):327-41.

Kliewer SA, Umesono K, Mangelsdorf DJ, Evans RM. Retinoid X receptor interacts with nuclear receptors in retinoic acid, thyroid hormone and vitamin D3 signalling. Nature. 1992 Jan 30;355(6359):446-9.

Koenig RJ. Thyroid hormone receptor coactivators and corepressors. Thyroid. 1998 Aug;8(8):703-13.

Koenderink GH, Dogic Z, Nakamura F, Bendix PM, MacKintosh FC, Hartwig JH, Stossel TP, Weitz DA. An active biopolymer network controlled by molecular motors. Proc Natl Acad Sci U S A. 2009 Sep 8;106(36):15192-7.

Kwan KY, Shen J, Corey DP. Multipotent inner-ear progenitor cells reveal a molecular switch from self-renewal to differentiation. (in preparation). SHIELD: Shared Harvard Inner-Ear Laboratory Database, https://shield.hms.harvard.edu/

Lahne M, Gale JE. Damage-induced activation of ERK1/2 in cochlear supporting cells is a hair cell death-promoting signal that depends on extracellular ATP and calcium. J Neurosci. 2008 May 7;28(19):4918-28.

Lanford PJ, Lan Y, Jiang R, Lindsell C, Weinmaster G, Gridley T, Kelley MW. Notch signalling pathway mediates hair cell development in mammalian cochlea. Nat Genet. 1999 Mar;21(3):289-92.

Lee YS, Liu F, Segil N. A morphogenetic wave of p27Kip1 transcription directs cell cycle exit during organ of Corti development. Development. 2006 Aug;133(15):2817-26.

Levayer R, Lecuit T. Biomechanical regulation of contractility: spatial control and dynamics. Trends Cell Biol. 2012 Feb;22(2):61-81.

Li C, Scott DA, Hatch E, Tian X, Mansour SL. Dusp6 (Mkp3) is a negative feedback regulator of FGF-stimulated ERK signaling during mouse development. Development. 2007 Jan;134(1):167-76.

Lieleg O, Claessens MM, Luan Y, Bausch AR. Transient binding and dissipation in cross-linked actin networks. Phys Rev Lett. 2008 Sep 5;101(10):108101.

Lim DJ, Anniko M. Developmental morphology of the mouse inner ear. A scanning electron microscopic observation. Acta Otolaryngol Suppl. 1985;422:1-69.

Lin CC, Melo FA, Ghosh R, Suen KM, Stagg LJ, Kirkpatrick J, Arold ST, Ahmed Z, Ladbury JE. Inhibition of basal FGF receptor signaling by dimeric Grb2. Cell. 2012 Jun 22;149(7):1514-24.

Liu Z, Dearman JA, Cox BC, Walters BJ, Zhang L, Ayrault O, Zindy F, Gan L, Roussel MF, Zuo J. Age-dependent in vivo conversion of mouse cochlear pillar and Deiters' cells to immature hair cells by Atoh1 ectopic expression. J Neurosci. 2012 May 9;32(19):6600-10.

Lennon AM, Esfandiari A, Gavaret JM, Courtin F, Pierre M. 12-O-tetradecanoylphorbol 13-acetate and fibroblast growth factor increase the 30-kDa substrate binding subunit of type II deiodinase in astrocytes. J Neurochem. 1994 Jun;62(6):2116-23.

Leonova EV, Raphael Y. Organization of cell junctions and cytoskeleton in the reticular lamina in normal and ototoxically damaged organ of Corti. Hear Res. 1997 Nov;113(1-2):14-28.

Lewis J. Neurogenic genes and vertebrate neurogenesis. Curr Opin Neurobiol. 1996 Feb;6(1):3-10.

Loubière LS, Vasilopoulou E, Bulmer JN, Taylor PM, Stieger B, Verrey F, McCabe CJ, Franklyn JA, Kilby MD, Chan SY. Expression of thyroid hormone transporters in the human placenta and changes associated with intrauterine growth restriction. Placenta. 2010 Apr;31(4):295-304. Epub 2010 Feb 18.

Love AEH. Boussinesq's problem for a rigid cone. Quart Jour Math. 1939 10:161-75.

Ma X, Jana SS, Conti MA, Kawamoto S, Claycomb WC, Adelstein RS. Ablation of nonmuscle myosin II-B and II-C reveals a role for nonmuscle myosin II in cardiac myocyte karyokinesis. Mol Biol Cell. 2010 Nov 15;21(22):3952-62.

Mangasarian K, Li Y, Mansukhani A, Basilico C. Mutation associated with Crouzon syndrome causes ligand-independent dimerization and activation of FGF receptor-2. J Cell Physiol. 1997 Jul;172(1):117-25.

Mason I. Initiation to end point: the multiple roles of fibroblast growth factors in neural development. Nat Rev Neurosci. 2007 Aug;8(8):583-96.

Matsui JI, Gale JE, Warchol ME. Critical signaling events during the aminoglycoside-induced death of sensory hair cells in vitro. J Neurobiol. 2004 Nov;61(2):250-66.

Matsushita T, Wilcox WR, Chan YY, Kawanami A, Bükülmez H, Balmes G, Krejci P, Mekikian PB, Otani K, Yamaura I, Warman ML, Givol D, Murakami S. FGFR3 promotes synchondrosis closure and fusion of ossification centers through the MAPK pathway. Hum Mol Genet. 2009 Jan 15;18(2):227-40.

McKinnon B, Li H, Richard K, Mortimer R. Synthesis of thyroid hormone binding proteins transthyretin and albumin by human trophoblast. J Clin Endocrinol Metab. 2005 Dec;90(12):6714-20.

Merchant SN, Burgess BJ, Adams JC, Kashtan CE, Gregory MC, Santi PA, Colvin R, Collins B, Nadol JB Jr. Temporal bone histopathology in alport syndrome. Laryngoscope. 2004 Sep;114(9):1609-18.

Miller RK, Heller KK, Frisèn L, Wallack DL, Loayza D, Gammie AE, Rose MD. The kinesin-related proteins, Kip2p and Kip3p, function differently in nuclear migration in yeast. Mol Biol Cell. 1998 Aug;9(8):2051-68.

Mimori-Kiyosue Y, Grigoriev I, Lansbergen G, Sasaki H, Matsui C, Severin F, Galjart N, Grosveld F, Vorobjev I, Tsukita S, Akhmanova A. CLASP1 and CLASP2 bind to

EB1 and regulate microtubule plus-end dynamics at the cell cortex. J Cell Biol 2005; 168:141-53.

Mitchison TJ, Salmon ED. Mitosis: a history of division. Nat Cell Biol. 2001 Jan;3(1):E17-21.

Montcouquiol M, Kelley MW. Planar and vertical signals control cellular differentiation and patterning in the mammalian cochlea. J Neurosci. 2003 Oct 15;23(28):9469-78.

Morín M, Bryan KE, Mayo-Merino F, Goodyear R, Mencía A, Modamio-Høybjør S, del Castillo I, Cabalka JM, Richardson G, Moreno F, Rubenstein PA, Moreno-Pelayo MA. In vivo and in vitro effects of two novel gamma-actin (ACTG1) mutations that cause DFNA20/26 hearing impairment. Hum Mol Genet. 2009 Aug 15;18(16):3075-89.

Morrison A, Hodgetts C, Gossler A, Hrabé de Angelis M, Lewis J. Expression of Delta1 and Serrate1 (Jagged1) in the mouse inner ear. Mech Dev. 1999 Jun;84(1-2):169-72.

Mortimer RH, Landers KA, Balakrishnan B, Li H, Mitchell MD, Patel J, Richard K. Secretion and transfer of the thyroid hormone binding protein transthyretin by human placenta. Placenta. 2012 Apr;33(4):252-6.

Mueller KL, Jacques BE, Kelley MW. Fibroblast growth factor signaling regulates pillar cell development in the organ of corti. J Neurosci. 2002 Nov 1;22(21):9368-77.

Ng L, Goodyear RJ, Woods CA, Schneider MJ, Diamond E, Richardson GP, Kelley MW, Germain DL, Galton VA, Forrest D. Hearing loss and retarded cochlear development in mice lacking type 2 iodothyronine deiodinase. Proc Natl Acad Sci U S A. 2004 Mar 9;101(10):3474-9.

Ng L, Hernandez A, He W, Ren T, Srinivas M, Ma M, Galton VA, St Germain DL, Forrest D. A protective role for type 3 deiodinase, a thyroid hormone-inactivating enzyme, in cochlear development and auditory function. Endocrinology. 2009 Apr;150(4):1952-60.

Novak P, Li C, Shevchuk AI, Stepanyan R, Caldwell M, Hughes S, Smart TG, Gorelik J, Ostanin VP, Lab MJ, Moss GW, Frolenkov GI, Klenerman D, Korchev YE. Nanoscale live-cell imaging using hopping probe ion conductance microscopy. Nat Methods. 2009 Apr;6(4):279-81.

O'Shea PJ, Guigon CJ, Williams GR, Cheng SY. Regulation of fibroblast growth factor receptor-1 (FGFR1) by thyroid hormone: identification of a thyroid hormone response element in the murine Fgfr1 promoter. Endocrinology. 2007 Dec;148(12):5966-76.

Okano Y, Iwai H. Effect of the high potassium medium on cultured cochlear epithelial cells. Arch Otorhinolaryngol. 1975;209(2):121-5.

Olsen SK, Ibrahimi OA, Raucci A, Zhang F, Eliseenkova AV, Yayon A, Basilico C, Linhardt RJ, Schlessinger J, Mohammadi M. Insights into the molecular basis for fibroblast growth factor receptor autoinhibition and ligand-binding promiscuity. Proc Natl Acad Sci U S A. 2004 Jan 27;101(4):935-40.

Olson DP, Sun B, Koenig RJ. Thyroid hormone response element architecture affects corepressor release from thyroid hormone receptor dimers. J Biol Chem. 1998 Feb 6;273(6):3375-80.

Olson ES, Mountain DC. Mapping the cochlear partition's stiffness to its cellular architecture. J Acoust Soc Am. 1994 Jan;95(1):395-400.

Ornitz DM. FGFs, heparan sulfate and FGFRs: complex interactions essential for development. Bioessays. 2000 Feb;22(2):108-12.

Orvidas LJ, Fabry LB, Diacova S, McDonald TJ. Hearing and otopathology in Crouzon syndrome. Laryngoscope. 1999 Sep;109(9):1372-5.

Oshima K, Shin K, Diensthuber M, Peng AW, Ricci AJ, Heller S. Mechanosensitive hair cell-like cells from embryonic and induced pluripotent stem cells. Cell. 2010 May 14;141(4):704-16.

Patel J, Landers K, Li H, Mortimer RH, Richard K. Delivery of maternal thyroid hormones to the fetus. Trends Endocrinol Metab. 2011 May;22(5):164-70.

Perrin BJ, Sonnemann KJ, Ervasti JM. Beta-actin and Gamma-actin are each dispensable for auditory hair cell development but required for Stereocilia maintenance. PLoS Genet. 2010 Oct 14;6(10):e1001158.

Petralia RS, Wenthold RJ. Light and electron immunocytochemical localization of AMPA-selective glutamate receptors in the rat brain. J Comp Neurol. 1992 Apr 15;318(3):329-54.

Pickles JO. The expression of fibroblast growth factors and their receptors in the embryonic and neonatal mouse inner ear. Hear Res. 2001 May;155(1-2):54-62.

Piedrafita FJ, Bendik I, Ortiz MA, Pfahl M. Thyroid hormone receptor homodimers can function as ligand-sensitive repressors. Mol Endocrinol. 1995 May;9(5):563-78.

Pirvola U, Cao Y, Oellig C, Suoqiang Z, Pettersson RF, Ylikoski J. The site of action of neuronal acidic fibroblast growth factor is the organ of Corti of the rat cochlea. Proc Natl Acad Sci U S A. 1995 Sep 26;92(20):9269-73.

Pirvola U, Spencer-Dene B, Xing-Qun L, Kettunen P, Thesleff I, Fritzsch B, Dickson C, Ylikoski J. FGF/FGFR-2(IIIb) signaling is essential for inner ear morphogenesis. J Neurosci. 2000 Aug 15;20(16):6125-34.

Pirvola U, Ylikoski J, Trokovic R, Hébert JM, McConnell SK, Partanen J. FGFR1 is required for the development of the auditory sensory epithelium. Neuron. 2002 Aug 15;35(4):671-80.

Puligilla C, Feng F, Ishikawa K, Bertuzzi S, Dabdoub A, Griffith AJ, Fritzsch B, Kelley MW. Disruption of fibroblast growth factor receptor 3 signaling results in defects in cellular differentiation, neuronal patterning, and hearing impairment. Dev Dyn. 2007 Jul;236(7):1905-17.

Puligilla C, Dabdoub A, Brenowitz SD, Kelley MW. Sox2 induces neuronal formation in the developing mammalian cochlea. J Neurosci. 2010 Jan 13;30(2):714-22.

Radde-Gallwitz K, Pan L, Gan L, Lin X, Segil N, Chen P. Expression of Islet1 marks the sensory and neuronal lineages in the mammalian inner ear. J Comp Neurol. 2004 Sep 27;477(4):412-21.

Rasband, W.S., ImageJ, U. S. National Institutes of Health, Bethesda, Maryland, USA, http://imagej.nih.gov/ij/, 1997-2012.

Ribeiro RC, Feng W, Wagner RL, Costa CH, Pereira AC, Apriletti JW, Fletterick RJ, Baxter JD. Definition of the surface in the thyroid hormone receptor ligand binding domain for association as homodimers and heterodimers with retinoid X receptor. J Biol Chem. 2001 May 4;276(18):14987-95.

Richardson GP, Forge A, Kros CJ, Fleming J, Brown SD, Steel KP. Myosin VIIA is required for aminoglycoside accumulation in cochlear hair cells. J Neurosci. 1997 Dec 15;17(24):9506-19.

Ruben RJ. Development of the inner ear of the mouse: a radioautographic study of terminal mitoses. Acta Otolaryngol. 1967:Suppl 220:1-44.

Rüsch A, Ng L, Goodyear R, Oliver D, Lisoukov I, Vennstrom B, Richardson G, Kelley MW, Forrest D. Retardation of cochlear maturation and impaired hair cell function caused by deletion of all known thyroid hormone receptors. J Neurosci. 2001 Dec 15;21(24):9792-800.

Russell IJ, Richardson GP, Cody AR. Mechanosensitivity of mammalian auditory hair cells in vitro. Nature. 1986 May 29-Jun 4;321(6069):517-9.

Russell IJ, Richardson GP. The morphology and physiology of hair cells in organotypic cultures of the mouse cochlea. Hear Res. 1987 Nov;31(1):9-24.

Sage C, Huang M, Karimi K, Gutierrez G, Vollrath MA, Zhang DS, García-Añoveros J, Hinds PW, Corwin JT, Corey DP, Chen ZY. Proliferation of functional hair cells in vivo in the absence of the retinoblastoma protein. Science. 2005 Feb 18;307(5712):1114-8.

Sap J, de Magistris L, Stunnenberg H, Vennström B. A major thyroid hormone response element in the third intron of the rat growth hormone gene. EMBO J. 1990 Mar;9(3):887-96.

Sapir T, Shmueli A, Levy T, Timm T, Elbaum M, Mandelkow EM, Reiner O. Antagonistic effects of doublecortin and MARK2/Par-1 in the developing cerebral cortex. J Neurosci 2008; 28:13008-13.

Sato T, Doi K, Taniguchi M, Yamashita T, Kubo T, Tohyama M. Progressive hearing loss in mice carrying a mutation in the p75 gene. Brain Res. 2006 May 26;1091(1):224-34.

Schneider MJ, Fiering SN, Pallud SE, Parlow AF, St Germain DL, Galton VA. Targeted disruption of the type 2 selenodeiodinase gene (DIO2) results in a phenotype of pituitary resistance to T4. Mol Endocrinol. 2001 Dec;15(12):2137-48.

Schneider MJ, Fiering SN, Thai B, Wu SY, St Germain E, Parlow AF, St Germain DL, Galton VA. Targeted disruption of the type 1 selenodeiodinase gene (Dio1) results in marked changes in thyroid hormone economy in mice. Endocrinology. 2006 Jan;147(1):580-9.

Schweizer U, Köhrle J. Function of thyroid hormone transporters in the central nervous system. Biochim Biophys Acta. 2012 Aug 7.

Scott S. Sections of the Human Cochlea through the Organ of Corti, showing Beaded Nerve-fibril traversing the Tunnel of Corti, and Cell Fibrillae projecting from the Hair-cells. Proc R Soc Med. 1909;2(Otol Sect):29-34.

Sen S, Subramanian S, Discher DE. Indentation and adhesive probing of a cell membrane with AFM: theoretical model and experiments. Biophys J. 2005 Nov;89(5):3203-13.

Sharlin DS, Visser TJ, Forrest D. Developmental and cell-specific expression of thyroid hormone transporters in the mouse cochlea. Endocrinology. 2011 Dec;152(12):5053-64.

Shimokawa K, Kimura-Yoshida C, Nagai N, Mukai K, Matsubara K, Watanabe H, Matsuda Y, Mochida K, Matsuo I. Cell surface heparan sulfate chains regulate local reception of FGF signaling in the mouse embryo. Dev Cell. 2011 Aug 16;21(2):257-72.

Shinya M, Koshida S, Sawada A, Kuroiwa A, Takeda H. Fgf signalling through MAPK cascade is required for development of the subpallial telencephalon in zebrafish embryos. Development. 2001 Nov;128(21):4153-64.

Simonneau L, Gallego M, Pujol R. Comparative expression patterns of T-, N-, E-cadherins, beta-catenin, and polysialic acid neural cell adhesion molecule in rat cochlea during development: implications for the nature of Kölliker's organ. J Comp Neurol. 2003 Apr 28;459(2):113-26.

Sjöberg M, Vennström B. Ligand-dependent and -independent transactivation by thyroid hormone receptor beta 2 is determined by the structure of the hormone response element. Mol Cell Biol. 1995 Sep;15(9):4718-26.

Slepecky N, Chamberlain SC. Tropomyosin co-localizes with actin microfilaments and microtubules within supporting cells of the inner ear. Cell Tissue Res. 1987 Apr;248(1):63-6.

Slepecky NB, Henderson CG, Saha S. Post-translational modifications of tubulin suggest that dynamic microtubules are present in sensory cells and stable microtubules are present in supporting cells of the mammalian cochlea. Hear Res. 1995 Nov;91(1-2):136-47.

Slepecky NB. Structure of the Mammalian Cochlea. The Cochlea. Springer Handbook of Auditory Research. 1996, 8:44-129.

Sneddon IN. The relation between load and penetration in the axisymmetric Boussinesq problem for a punch of arbitrary profile. Int. J. Eng. Sci. 1965 3:47.

Soilu-Hänninen M, Ekert P, Bucci T, Syroid D, Bartlett PF, Kilpatrick TJ. Nerve growth factor signaling through p75 induces apoptosis in Schwann cells via a Bcl-2-independent pathway. J Neurosci. 1999 Jun 15;19(12):4828-38.

Songyang Z, Shoelson SE, Chaudhuri M, Gish G, Pawson T, Haser WG, King F, Roberts T, Ratnofsky S, Lechleider RJ, et al. SH2 domains recognize specific phosphopeptide sequences. Cell. 1993 Mar 12;72(5):767-78.

Souter M, Nevill G, Forge A. Postnatal maturation of the organ of Corti in gerbils: morphology and physiological responses. J Comp Neurol. 1997 Oct 6;386(4):635-51.

Stavridis MP, Lunn JS, Collins BJ, Storey KG. A discrete period of FGF-induced Erk1/2 signalling is required for vertebrate neural specification. Development. 2007 Aug;134(16):2889-94.

Stepanyan R, Belyantseva IA, Griffith AJ, Friedman TB, Frolenkov GI. Auditory mechanotransduction in the absence of functional myosin-XVa. J Physiol. 2006 Nov 1;576(Pt 3):801-8.

Sundararaghavan HG, Burdick JA. Gradients with depth in electrospun fibrous scaffolds for directed cell behavior. Biomacromolecules. 2011 Jun 13;12(6):2344-50.

Taleb M, Brandon CS, Lee FS, Lomax MI, Dillmann WH, Cunningham LL. Hsp70 inhibits aminoglycoside-induced hair cell death and is necessary for the protective effect of heat shock. J Assoc Res Otolaryngol. 2008 Sep;9(3):277-89. Epub 2008 May 30.

Tannenbaum J, Slepecky NB. Localization of microtubules containing posttranslationally modified tubulin in cochlear epithelial cells during development. Cell Motil Cytoskeleton. 1997;38(2):146-62.

Tolomeo JA, Holley MC. Mechanics of microtubule bundles in pillar cells from the inner ear. Biophys J. 1997 Oct;73(4):2241-7.

Tolomeo JA, Steele CR, Holley MC. Mechanical properties of the lateral cortex of mammalian auditory outer hair cells. Biophys J. 1996 Jul;71(1):421-9.

Toyama K, Ozeki M, Hamajima Y, Lin J. Expression of the integrin genes in the developing cochlea of rats. Hear Res. 2005 Mar;201(1-2):21-6.

Tullio AN, Accili D, Ferrans VJ, Yu ZX, Takeda K, Grinberg A, Westphal H, Preston YA, Adelstein RS. Nonmuscle myosin II-B is required for normal development of the mouse heart. Proc Natl Acad Sci U S A. 1997 Nov 11;94(23):12407-12.

Umesono K, Murakami KK, Thompson CC, Evans RM. Direct repeats as selective response elements for the thyroid hormone, retinoic acid, and vitamin D3 receptors. Cell. 1991 Jun 28;65(7):1255-66.

Vitre B, Coquelle FM, Heichette C, Garnier C, Chrétien D, Arnal I. EB1 regulates microtubule dynamics and tubulin sheet closure in vitro. Nat Cell Biol. 2008; 10:415-21.

von Békésy G. Current status of theories of hearing. Science. 1956 May 4;123(3201):779-83.

Weitzel JM. To bind or not to bind - how to down-regulate target genes by liganded thyroid hormone receptor? Thyroid Res. 2008 Oct 11;1(1):4.

Welch BL. The generalization of "Student's" problem when several different population variances are involved. Biometrika. 1947 34(1-2):28-35.

Wikström L, Johansson C, Saltó C, Barlow C, Campos Barros A, Baas F, Forrest D, Thorén P, Vennström B. Abnormal heart rate and body temperature in mice lacking thyroid hormone receptor alpha 1. EMBO J. 1998 Jan 15;17(2):455-61.

Witte MC, Montcouquiol M, Corwin JT. Regeneration in avian hair cell epithelia: identification of intracellular signals required for S-phase entry. Eur J Neurosci. 2001 Sep;14(5):829-38.

Wloga D, Gaertig J. Post-translational modifications of microtubules. J Cell Sci. 2010 Oct 15;123(Pt 20):3447-55.

Yamamoto N, Okano T, Ma X, Adelstein RS, Kelley MW. Myosin II regulates extension, growth and patterning in the mammalian cochlear duct. Development. 2009 Jun;136(12):1977-86.

Yim EK, Darling EM, Kulangara K, Guilak F, Leong KW. Nanotopography-induced changes in focal adhesions, cytoskeletal organization, and mechanical properties of human mesenchymal stem cells. Biomaterials. 2010 Feb;31(6):1299-306.

Yoshida A, Yamamoto N, Kinoshita M, Hiroi N, Hiramoto T, Kang G, Trimble WS, Tanigaki K, Nakagawa T, Ito J. Localization of septin proteins in the mouse cochlea. Hear Res. 2012 Jul;289(1-2):40-51.

Yu VC, Delsert C, Andersen B, Holloway JM, Devary OV, Näär AM, Kim SY, Boutin JM, Glass CK, Rosenfeld MG. RXR beta: a coregulator that enhances binding of retinoic acid, thyroid hormone, and vitamin D receptors to their cognate response elements. Cell. 1991 Dec 20;67(6):1251-66.

Zagadou BF, Mountain DC. Analysis of the cochlear amplifier fluid pump hypothesis. J Assoc Res Otolaryngol. 2012 Apr;13(2):185-97.

Zhu M, Yang T, Wei S, DeWan AT, Morell RJ, Elfenbein JL, Fisher RA, Leal SM, Smith RJ, Friderici KH. Mutations in the gamma-actin gene (ACTG1) are associated with dominant progressive deafness (DFNA20/26). Am J Hum Genet. 2003 Nov;73(5):1082-91.

7 APPENDIX I

For each force-distance curve, Young's modulus was estimated with a non-linear least-squared fit to Sneddon's model for an indenting cone (Sneddon, 1965):

$$F = (2 \tan \theta)/\pi * \frac{E}{(1 - \nu^2)} \delta^2$$

where F is the applied force, δ is the indentation, α is the half-angle of the cone and assumed to be 35˚, and Poisson's ratio (υ) is assumed to be 0.5. Force is expressed in terms of cantilever deflection (*d*) and cantilever spring constant (*k*) as:

$$F = kd$$

The indentation, δ, is calculated as:

$$\delta = (\mathrm{Z} - \mathrm{Z}_0) - d$$

where Z is the distance of the piezo displacement of the cantilever and Z_0 is the piezo distance at the contact point.